Author Manuscript
Author Manuscript
Author Manuscript
Author Manuscript

HHS Public Access
Author manuscript
Cell Rep. Author manuscript; available in PMC 2023 October 23.

Published in final edited form as:
Cell Rep. 2023 June 27; 42(6): 112665. doi:10.1016/j.celrep.2023.112665.

ETV2 primes hematoendothelial gene enhancers prior to hematoendothelial fate commitment

Jeffrey D. Steimle[1,8,9], **Chul Kim**[1,2,9], **Megan Rowton**[1], **Rangarajan D. Nadadur**[1], **Zhezhen Wang**[1], **Matthew Stocker**[1], **Andrew D. Hoffmann**[1], **Erika Hanson**[1], **Junghun Kweon**[1], **Tanvi Sinha**[5], **Kyunghee Choi**[6], **Brian L. Black**[5,7], **John M. Cunningham**[2], **Ivan P. Moskowitz**[1,10,*], **Kohta Ikegami**[3,4,10,11,*]

[1]Departments of Pediatrics, Pathology, and Human Genetics, University of Chicago, Chicago, IL 60637, USA

[2]Department of Pediatrics, Section of Hematology/Oncology, University of Chicago, Chicago, IL 60637, USA

[3]Division of Molecular and Cardiovascular Biology, Cincinnati Children's Hospital Medical Center, Cincinnati, OH 45229, USA

[4]Department of Pediatrics, University of Cincinnati, Cincinnati, OH 45229, USA

[5]Cardiovascular Research Institute, University of California, San Francisco, San Francisco, CA 94143, USA

[6]Department of Pathology and Immunology, Washington University School of Medicine, St. Louis, MO 63110, USA

[7]Department of Biochemistry and Biophysics, University of California, San Francisco, San Francisco, CA 94143, USA

[8]Present address: Department of Integrative Physiology, Baylor College of Medicine, Houston, TX 77030, USA

[9]These authors contributed equally

[10]These authors contributed equally

[11]Lead contact

SUMMARY

This is an open access article under the CC BY-NC-ND license (http://creativecommons.org/licenses/by-nc-nd/4.0/).

*Correspondence: imoskowitz@uchicago.edu (I.P.M.), kohta.ikegami@cchmc.org (K.I.).

AUTHOR CONTRIBUTIONS

Conceptualization, J.D.S., C.K., I.P.M., and K.I.; methodology, C.K., I.P.M., and K.I.; formal analysis, J.D.S., Z.W., and K.I.; investigation, C.K., R.D.N., A.D.H., E.H., M.R., M.S., and J.K.; resources, K.C.; data curation, J.D.S. and K.I.; writing – original draft, J.D.S., I.P.M., and K.I.; writing – review & editing, J.D.S., T.S., K.C., B.L.B., I.P.M., and K.I.; visualization, J.D.S. and K.I.; supervision, J.M.C., I.P.M., and K.I.; project administration, I.P.M. and K.I.; funding acquisition, J.M.C., I.P.M., and K.I.

DECLARATION OF INTERESTS

The authors declare no competing interests.

SUPPLEMENTAL INFORMATION

Supplemental information can be found online at https://doi.org/10.1016/j.celrep.2023.112665.

Author Manuscript Author Manuscript Author Manuscript Author Manuscript

Mechanisms underlying distinct specification, commitment, and differentiation phases of cell fate determination remain undefined due to difficulties capturing these processes. Here, we interrogate the activity of ETV2, a transcription factor necessary and sufficient for hematoendothelial differentiation, within isolated fate intermediates. We observe transcriptional upregulation of *Etv2* and opening of ETV2-binding sites, indicating new ETV2 binding, in a common cardiac-hematoendothelial progenitor population. Accessible ETV2-binding sites are active at the *Etv2* locus but not at other hematoendothelial regulator genes. Hematoendothelial commitment coincides with the activation of a small repertoire of previously accessible ETV2-binding sites at hematoendothelial regulators. Hematoendothelial differentiation accompanies activation of a large repertoire of new ETV2-binding sites and upregulation of hematopoietic and endothelial gene regulatory networks. This work distinguishes specification, commitment, and sublineage differentiation phases of ETV2-dependent transcription and suggests that the shift from ETV2 binding to ETV2-bound enhancer activation, not ETV2 binding to target enhancers, drives hematoendothelial fate commitment.

In brief

Mechanisms driving the specification, commitment, and differentiation phases of fate determination remain elusive. Steimle et al. investigate the activity of the hematoendothelial master transcription factor ETV2 and identify that the shift from ETV2 binding to ETV2-bound enhancer activation, not ETV2 binding to target enhancers, drives hematoendothelial fate commitment.

Graphical Abstract

Author Manuscript Author Manuscript Author Manuscript Author Manuscript

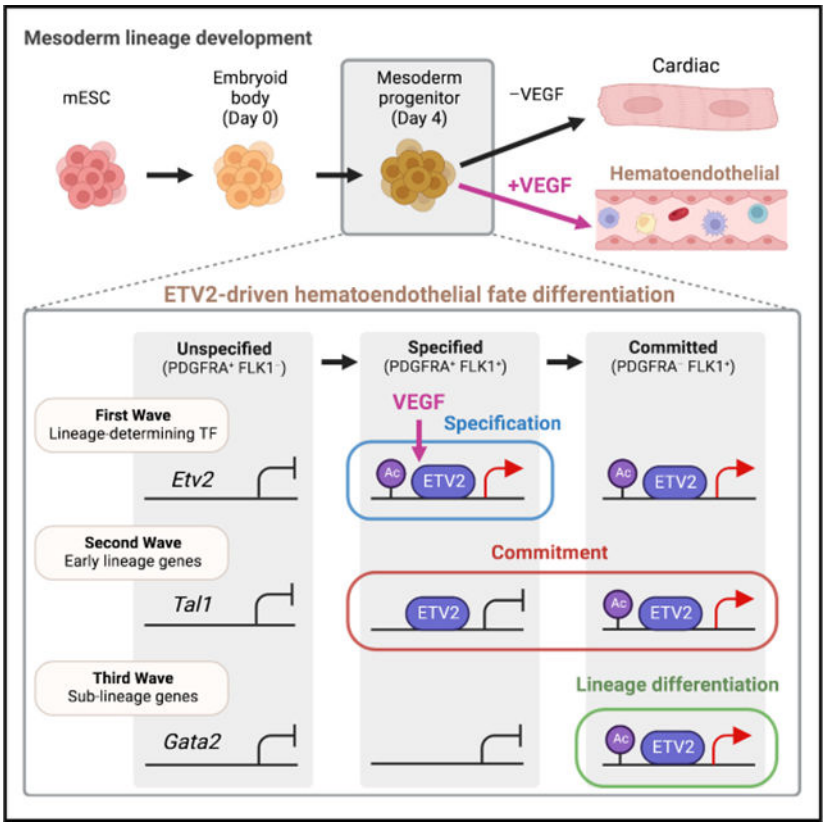

INTRODUCTION

Successive cell fate decisions underpin the development of multicellular organisms.[1–3] Transcription factors (TFs) play a central role in fate decisions by binding *cis*-regulatory elements and directing fate-specific transcriptional and chromatin states.[4–6] The transcriptional mechanisms that drive cell fate transitions are an area of active investigation.[7–9] Individual cells undergoing fate transition often display a mixture of progenitor and destination transcriptional and chromatin states.[7,10–12] One example is a phenomenon described as lineage priming, in which progenitor cells exhibit a subset of transcriptional and chromatin states characteristic of destination cells.[13–16] However, the mechanisms that drive transcriptional and chromatin state changes during fate transition processes remain unresolved, in part due to difficulties isolating and interrogating specific intermediates during cell fate decisions.

An early common mesoderm progenitor generates both the cardiac lineage for heart development and the hematoendothelial lineage for hematopoiesis and vasculogenesis.[17–28] Vascular endothelial growth factor (VEGF) reception by FLK1 (VEGFR2, *Kdr*) induces hematoendothelial fate specification by transcriptionally activating *Etv2*,[29–31] an Ets-family, lineage-determining TF for the vertebrate hematoendothelial lineage.[29,32–41] *Etv2* expression in FLK1$^+$ mesoderm specifies the hematoendothelial lineage at the expense of the cardiac lineage cell autonomously.[42,43]

Author Manuscript Author Manuscript Author Manuscript Author Manuscript

In this study, we investigate dynamics of transcription, chromatin accessibility, and enhancer activity in specification, commitment, and differentiation phases of hematoendothelial development by examining fate intermediates originating from single time points of mouse embryonic stem cell (mESC) differentiation. This allows the distinct transcriptional mechanisms distinguishing specification, commitment, and sublineage differentiation phases of hematoendothelial gene expression to be delivered.

RESULTS

Sequential derivation of PDGFRα - and FLK1-expressing mesoderm populations

During vertebrate development, PDGFRα$^+$ FLK1$^+$ (*PF*) cells are defined as multipotent cardiovascular progenitors with cardiac and hematoendothelial potential.[24,25] Previous work delineated the fates derived from PDGFRα$^+$ and/or FLK1$^+$ populations from mESC differentiation using a serum-free medium containing activin A, BMP4, and VEGF (ABV) (Figure 1A).[24,25] We observed that 100% of the PDGFRα$^+$ populations were mesoderm, only the *PF* population generated cardiomyocytes, and only the PDGFRα$^-$ FLK1$^+$ (F) population formed blood colonies (Figures 1A–1D and S1A–S1D).[24,25] These observations confirmed that the *PF* population defined a cardiomyogenic progenitor and the *F* population a hematoendothelial progenitor and that the PDGFRα$^+$ FLK1$^-$ (*P*) population lacked both potentials.[24,25,29]

We performed a time course study to define the emergence of PDGFRα/FLK1 subpopulations. Cells were initially PDGFRα$^-$ FLK1$^-$ (*P*–*F*–) at day 2.5. The *P* population emerged at day 3, followed by *PF* at day 3.125, and finally *F* at day 3.5 (Figures 1E and S1E). Differentiation of isolated PDGFRα/FLK1 subpopulations confirmed this order of differentiation (Figure S1F). Thus, the *P* population was an early multipotent mesodermal progenitor that gave rise to *PF*, a common cardiomyogenic/hematoendothelial progenitor, which could differentiate into cardiomyocytes upon isolation from ABV or into the hematoendothelial *F* population if retained in ABV (Figure 1F).

We confirmed previous observations that VEGF signaling is required for hematoendothelial commitment, driving the transition from *PF* to *F* (Figures 1G and 1H).[21–23,29] However, mESC differentiation with or without VEGF generated the *PF* population or *PF*-derived cardiomyocytes with comparable efficiency (Figures 1G–1I). Thus, VEGF was dispensable for generating the common cardiac/hematoendothelial *PF* population but was required for the hematoendothelial commitment in the *PF*-to-*F* transition.

Two distinct waves of hematoendothelial gene activation

The resolution of PDGFRα/FLK1 fate potentials allowed us to investigate mechanisms driving the sequential phases of cardiomyogenic/hematoendothelial fate commitment. We first investigated gene expression differences between the *P*, *PF*, and *F* populations at day 4 of differentiation using RNA sequencing (RNA-seq) (Figures 1J, 1K, S1G, and S1H; Table S1). We identified a union set of 3,050 genes that were differentially expressed either between *P* and *PF*, between *PF* and *F*, or both and clustered them based on their expression dynamics (Figures S1I and S1J; Table S1). This process identified six distinct patterns of

Author Manuscript Author Manuscript Author Manuscript Author Manuscript

expression and revealed two waves of gene expression affiliated with hematoendothelial development (Figure 1L). The "first-wave" cluster contained genes upregulated during the *P*-to-*PF* transition and remained high in *F* (193 genes) (Figure 1M). This cluster was overrepresented for Gene Ontology (GO) terms related to hematoendothelial and cardiomyogenic fates (Figure 1N; Table S2) and TFs implicated in hematopoietic and cardiac development such as *Tbx3*, *Hand2*, and *Gata6*.[44,45] Interestingly, *Etv2*, the lineage-determining TF for the hematoendothelial fate, was included in this first-wave cluster (Figure 1M), despite the *PF* population not yet being committed to the hematoendothelial fate.

The "second-wave" cluster contained genes whose expression was low in *P* and *PF*, and upregulated during the *PF*-to-*F* transition, accompanying hematoendothelial commitment and differentiation (1,081 genes) (Figure 1L). This cluster was overrepresented by hematoendothelial GO terms (Figure 1N) and included regulators of hematoendothelial, hematopoietic, and endothelial differentiation (Figures 1M, S1K, and S1L). Overall, the dynamic changes in transcription were associated with phenotypic cell fates and a pattern of differentiation mirroring development *in vivo*, lending credence to the sequential emergence of fate intermediates inferred from their temporal emergence *in vitro* (Figure 1O).

VEGF induces *Etv2* in the *PF* population without large-scale hematoendothelial gene expression

The unexpected observation that *Etv2* is upregulated in *PF* led us to further interrogate *Etv2* expression dynamics (Figure 1M). *Etv2* was 26-fold upregulated in *PF* relative to *P* and then only 2-fold upregulated in *F* relative to *PF* (Figure 2A). *Etv2* was among the most upregulated TF genes during the *P*-to-*PF* transition and among the highest expressed TFs in *PF* (98th percentile; Figure S2A). *Etv2* was the only ETS-family TF upregulated in *PF* and affiliated with the first-wave gene cluster (Figures 2B and S2B). Using the published single-cell transcriptome for mESCs undergoing spontaneous differentiation,[46] we confirmed that *Etv2*-expressing individual cells increased from 35% among *P* to 71% among *PF* and plateaued at 74% among *F* (Figures 2C and S2C) and that *Etv2* mRNA abundance in individual cells increased from *P* to *PF* and then plateaued in *F* (Figure S2D). We further confirmed ETV2 protein reporter expression in 72% of the *PF* cells, increased from 33% of *P* and 8% of *P*–*F*– cells (Figure 2D). Together, these observations established that *Etv2* was a first-wave hematoendothelial gene that was strongly induced in *PF* and remained highly expressed in *F*.

We tested the hypothesis that VEGF drove *Etv2* transcription in *PF* by RNA-seq of *PF* derived with or without VEGF. Only 61 genes were differentially expressed between the treatments, including 48 upregulated "VEGF-induced" genes (Figure 2E; Table S1). The strongest VEGF-induced gene was *Etv2* (Figure 2E). Only 11 of the 48 VEGF-induced genes were first-wave genes, and *Etv2* was the only known early regulator of hematoendothelial specification (Figure 2F). In contrast, 27 of the 48 VEGF-induced genes were second-wave genes and were only weakly induced by VEGF in *PF* but strongly upregulated in *F*, including several well-known regulators of hematoendothelial specification (e.g., *Tal1*, *Lmo2*, and *Flt1*) (Figure 2F). This analysis indicated that VEGF strongly

Author Manuscript Author Manuscript Author Manuscript Author Manuscript

upregulated *Etv2* without activating other hematoendothelial genes in the *PF* population (Figure 2G).

Pervasive gains of chromatin accessibility at ETS TF motif sites in *PF* and *F*

We hypothesized that *Etv2* expression in *PF* primed the hematoendothelial gene regulatory network in *PF* for the subsequent activation in *F*. We sought to distinguish between two models: that the transition from *Etv2* expression to ETV2 binding at target genes coincides with the *PF*-to-*F* transition or that ETV2 binds and poises at the target genes in *PF* until the transition to *F*. To distinguish between these hypotheses, we measured genomewide chromatin accessibility in *P*, *PF*, and *F* by assay for transposase-accessible chromatin (ATAC)-seq (Figures 3A and 3B; Table S3). We identified a union set of 41,383 sites that were differentially accessible either between *P* and *PF*, between *PF* and *F*, or both. These sites were predominantly distal to gene transcription start sites (96% ≥ 2 kb transcription start site [TSS]; Figure S3A). We clustered them based on their accessibility dynamics into 5 clusters (Figures S3B and S3C; Table S3). The enriched TF motifs within each cluster were consistent with the developmental gene expression patterns of the TFs observed in analogous gene expression clusters (Figures 3C and 3D). Specifically, we identified first- and second-wave alterations in chromatin accessibility that mirrored the sequential waves of hematoendothelial gene expression. First-wave ATAC sites (3,223) opened in the *P*-to-*PF* transition and remained open in *F*, whereas second-wave ATAC sites (19,534) were closed in *P* and *PF* and opened in the *PF*-to-*F* transition (Figure 3C). Both the first- and second-wave ATAC sites were most strongly overrepresented for the ETS motif (Figure 3D). Overrepresentation of the ETS motif in the first-wave ATAC sites supported the hypothesis that *Etv2* expression resulted in first-wave ETV2 binding in *PF*, despite the absence of large-scale hematoendothelial gene activation. Second-wave ETS motif enrichment suggested that first- and second-wave ETV2-binding events may distinguish different stages of hematoendothelial development.

VEGF dependence and TF footprinting support differential ETV2 binding in *PF* and *F*

We hypothesized that the observed gains of chromatin accessibility at ETS motif sites in *PF* indicated ETV2 binding induced by VEG*F*, as VEGF induced *Etv2* expression in *PF* (Figure 2E). To test this hypothesis, we profiled the chromatin accessibility by ATAC-seq in *PF* derived with (*PF*) or without VEGF (PF^{-VEGF}). Only 318 sites showed higher and 388 sites showed lower accessibility in *PF* relative to PF^{-VEGF}, respectively (Figure S3D; Table S3). The 318 sites with higher accessibility, but not the 388 sites with lower accessibility, were overrepresented for the ETS-family motif (Figures S3E and S3F), supporting the hypothesis that VEGF-driven *Etv2* expression resulted in ETV2 binding in *PF*.

We next investigated whether ETS motif sites in first- and second-wave ATAC sites exhibited TF footprinting.[47,48] At the ETV2 motif sites within the first-wave ATAC sites, footprints were undetectable in *P* but emerged in *PF* and remained present in *F* (Figure 3E). Therefore, at the first-wave ATAC sites, an ETS TF likely bound the ETV2 motif in *PF* and remained bound in *F*. At the second-wave ATAC sites, footprints were absent in both *P* and *PF*, but strongly emerged in *F*, suggesting *de novo* TF binding at ETV2 motifs in *F*. Because ETV2 is the only VEGF-dependent ETS TF that was transcriptionally induced

Author Manuscript Author Manuscript Author Manuscript Author Manuscript

in *PF* (Figures 2B and 2F), we infer that the footprinting analysis reflects specific ETV2 binding. These observations indicated two waves of ETV2 binding events: the first wave starting in *PF*, and the second wave starting in *F*.

We utilized the distinction between first- and second-wave ATAC clusters to refine available ETV2 chromatin immunoprecipitation (ChIP)-seq datasets generated in mESC-derived ETV2-overexpressing FLK1$^+$ cells, which would include both *PF* and *F* populations (Table S4).[41] Of the 3,307 ETV2-binding sites identified in the FLK1$^+$ population, 218 ETV2-binding sites overlapped the first-wave ATAC sites ("first-wave ETV2-binding sites"), whereas 1,879 ETV2-binding sites overlapped the second-wave ATAC sites ("second-wave ETV2-binding sites") (Table S3; Figures 3F–3H). ETV2-binding sites were underrepresented in other types of dynamic ATAC sites (Figure S3G). These results suggested that ETV2 binds a select set of first-wave ETV2-binding sites in *PF*, prior to the hematoendothelial commitment, followed by a large set of second-wave ETV2 binding in *F*, upon hematoendothelial fate commitment (Figure 3I).

Three patterns of accessibility and activation dynamics at ETV2-binding sites

We hypothesized that ETV2 binding primed first-wave ETV2-binding sites in *PF* that became active only upon transition to the *F* population. We performed ChIP-seq for histone H3 lysine 27 acetylation (H3K27ac), a modification associated with active regulatory elements, in *PF* and PF^{-VEGF} from day 4 of differentiation and in *F* from day 5 of differentiation (Table S4, Figures S4A and S4B). Only 15 of the 218 first-wave ETV2-binding sites (7%), representing "early-active" first-wave ETV2-binding sites (Figures 4A and 4B), were marked with H3K27ac in *PF* (Figure 4A). This included one ETV2-binding site located at the *Etv2* locus itself (Figure 4C). VEGF promoted H3K27ac of these sites in *PF*, as all 15 sites showed higher H3K27ac levels in *PF* compared with PF^{-VEGF} (Figure S4C). H3K27ac-marked first-wave ETV2-binding sites increased to 63% in *F* (137 sites; Figures 4A–4C). We termed the 123 first-wave ETV2-binding sites that gained H3K27ac in *F* but not in *PF* "delayed-active" ETV2-binding sites. These results identified a highly selective set of early-active first-wave ETV2-binding sites that were accessible and marked with H3K27ac in *PF* and a large number of delayed-active ETV2-binding sites that were active in *PF* but acquired H3K27ac later in *F* (Figure 4B). This result supported the hypothesis that most first-wave ETV2-binding sites were poised and accessible in *PF* but only became active upon the transition to *F*.

The 1,644 second-wave ETV2-binding sites were almost all devoid of H3K27ac signals in *PF* (99%) (Figure 4A). However, in *F*, the H3K27ac-marked fraction increased to 37% (689 sites; Figures 4A–4C). This identified a large subset of second-wave ETV2-binding sites activated selectively in *F*, in synchrony with accessibility gains. We termed the 660 second-wave ETV2-binding sites that gained H3K27ac only in *F* "late-active" ETV2-binding sites (Figure 4B). Together, H3K27ac dynamics identified early-active first-wave ETV2-binding sites that became open and active in *PF*, delayed-active first-wave sites that became open in *PF* but active in *F*, and late-active second-wave ETV2-binding sites that became open and active in *F* (Figure 4B).

Author Manuscript Author Manuscript Author Manuscript Author Manuscript

Activation dynamics of ETV2-binding sites correlates with the hematoendothelial gene regulatory hierarchy

We hypothesized that the sequential ETV2 binding and activation of ETV2-binding sites might underlie the regulatory hierarchy governing hematoendothelial fate differentiation. To test this hypothesis, we linked the distinct dynamics of accessible ETV2-binding sites and gained H3K27ac with sequential waves of gene expression, specifically linking early-active ETV2-binding sites to first-wave genes and delayed-active and late-active ETV2-binding sites to second-wave genes (Figure S4D). Only 3 first-wave genes, including *Etv2*, linked to early-active ETV2-binding sites (Figure 4D).

The 38 second-wave genes linked to delayed-active ETV2-binding sites included early upstream regulators of the hematoendothelial gene regulatory network, including *Tal1* and *Sox7* (Figure 4D).[18,33,49,50] The delayed-active ETV2-binding sites at second-wave genes suggested selective priming of important early regulators of hematoendothelial development in *PF*. Other well-characterized *Etv2* targets were absent from this cohort.

The 155 second-wave genes linked to late-active ETV2-binding sites included many TFs for endothelial development such as *Fli1*, *Gata2*, and *Sox18* (Figure 4D). Furthermore, these genes were enriched for GO terms related to endothelial development, but not hematopoietic development (Figures 4E and S4E), suggesting that late-active ETV2 binding selectively activated the endothelial branch of the hematoendothelial gene regulatory network, as suggested previously.[33,51] Delayed-active and late-active ETV2-binding sites were also found at some first-wave genes (Figure S4F) and might contribute to the secondary upregulation or maintenance of first-wave gene expression in *F*. These data suggested that late-active ETV2-binding sites were associated with the upregulation of genes downstream of commitment but essential for sublineage-specific differentiation within the hematoendothelial lineage. Overall, this analysis identified three different stages of hematoendothelial development promoted by ETV2, specification in *PF*, commitment during *PF*-to-*F* transition, and differentiation in *F*, distinguished by the sequential regulation of ETV2 binding and ETV2-bound enhancer activation (Figure 4F).

DISCUSSION

ETV2 has been identified as a master regulator TF for the hematoendothelial lineage development.[40,52,53] Our observations that *Etv2* is strongly expressed and that ETV2-binding sites gain accessibility in the multipotent *PF* mesoderm progenitor prior to hematoendothelial fate commitment were unexpected. A recent study reported a pioneering activity of ETV2 capable of binding to nucleosomal DNA for chromatin opening.[54] We propose that ETV2 opens and primes the ETV2-target hematoendothelial gene enhancers in the multipotent *PF* progenitor prior to hematoendothelial lineage commitment (Figure 4F).

How ETV2 activates different classes of genes for hematoendothelial development has been an outstanding question. Our data suggest that a combination of the timing of ETV2 binding and the timing of ETV2-bound enhancer activation enables sequential ETV2-dependent gene activation. *Etv2* itself becomes activated early upon ETV2 binding. This observation is consistent with the previously described feedforward activation of *Etv2*,[55]

Author Manuscript Author Manuscript Author Manuscript Author Manuscript

through an early-active ETV2-binding site, which may contribute to strong *Etv2* expression in the *PF* population. Subsequent early activation of other essential early activators of hematoendothelial commitment, such as *Tal1* and *Sox7*, requires a transition from bound to bound and activated enhancers. Finally, a late wave of ETV2 binding occurs at several TFs essential for endothelial development, such as *Fli1*, *Gata2*, and *Sox18*. This work provides a mechanistic model for how a single lineage-determining TF can differentially regulate distinct phases of specification, commitment, and sublineage differentiation during cell fate differentiation.

Limitations of the study

By investigating fate intermediates originating from a single time point of mESC differentiation, this study captures molecular dynamics during fate transitions. This approach contrasts with the conventional approach that compares samples from different time points.[4,56] A limitation of our approach is that our data represent averages of transcriptional states, chromatin states, or fate potentials of cells within isolated populations. Single-cell approaches can resolve transcriptional and chromatin states of individual cells but can only map these states along inferred developmental time scales and do not allow for direct evaluation of the fate potentials of the cells under investigation.[10,57–59] Our approach enables unambiguous determination of temporal relationships between isolated populations and evaluation of their fate potential. Combining fate intermediate isolation with single-cell approaches may address the potential heterogeneity of cells within intermediate states.

STAR★METHODS

RESOURCE AVAILABILITY

Lead contact—Further information and requests for resources and reagents should be directed to and will be fulfilled by the lead contact, Kohta Ikegami (kohta.ikegami@cchmc.org).

Materials availability—Cell lines used in this study will be available upon request with a completed Materials Transfer Agreement.

Data and code availability

- RNA-seq and ATAC-seq data are available at GEO with an accession number GSE136692.
- This paper does not report original code.
- All data reported in this paper will be shared by the lead contact upon request. Any additional information required to reanalyze the data reported in this paper is available from the lead contact upon request.

EXPERIMENTAL MODEL AND STUDY PARTICIPANT DETAILS

Mouse embryonic stem cells—We used the ZX1 mouse embryonic stem cell (ESC) line[85] for transcriptome and chromatin analyses. We used the Bry-GFP mESC line[86] for characterization of mESC differentiation. These two mESC lines were indistinguishable

Author Manuscript Author Manuscript Author Manuscript Author Manuscript

in their pluripotent states and differentiation potentials. We used the mESC line mESC with a C-terminal TdTomato insertion at the *Etv2* locus and a heterozygous GFP knockin at the *Brachyury* locus for the analysis of ETV2 and BRACHYURY protein expression. mESCs were maintained in a serum-free and feeder-free culture system.[25,87–89] For ESC maintenance, Neurobasal medium (ThermoFisher Scientific Cat. 21103049) and DMEM/F12 (ThermoFisher Scientific Cat. 10565018) (1:1) were supplemented with 0.5x N-2 supplement (ThermoFisher Scientific Cat. 17502048), 0.5x B27 supplement (ThermoFisher Scientific Cat. 17504044), 1x penicillin-streptomycin (ThermoFisher Scientific Cat. 15140148), 2mM Glutamine (ThermoFisher Scientific Cat. A2916801), 150μM mono-thioglycerol (MilliporeSigma, Cat. M6145), 0.05% BSA (MilliporeSigma, Cat. A9576), 1000 unit Mouse LIF (MilliporeSigma Cat. ESG1106), 1 μM PD0325901 (Procell Cat. 04–0006-10), 3 μM CHIR99021 (Procell Cat. 04–0004-10). PD0325901 and CHIR99021 were removed 2 days before the initiation of differentiation.

METHOD DETAILS

Mesoderm induction—To initiate differentiation, ESCs were dissociated with TrypLE express (ThermoFisher Scientific) and cultured in a 3:1 mixture of IMDM (ThermoFisher Scientific Cat. 12440053) and Ham's F12 (ThermoFisher Scientific Cat. 11765054) medium supplemented with 0.5x N-2 supplement, 0.5x B27 supplement, 1x penicillin-streptomycin, 2mM Glutamine, 0.5 mM ascorbic acid (MilliporeSigma Cat. A4544), 450 μM mono-thioglycerol, 0.05% BSA at the density of 0.1 million cells per mL in a 10-cm Petri dish (Becton Dickenson) for inducing embryoid bodies.[24,25] After 48 h, the embryoid bodies (EBs) were dissociated with TrypLE express. For mesoderm induction, the dissociated EBs were re-aggregated in the ABV regimen, defined as the StemPro-34 SFM medium (ThermoFisher Scientific Cat. 10639011) supplemented with 2mM Glutamine, 0.5 mM ascorbic acid, 450 μM mono-thioglycerol, 200 μg/mL human transferrin (MilliporeSigma Cat. T8158), 6 ng/mL human bFGF (R&D systems Cat. 233FB), 1 ng/mL human BMP4 (R&D systems Cat. 314BP), 8 ng/mL human Activin A (R&D systems Cat. 338AC), 5 ng/mL mouse VEGF (R&D systems Cat. 494MV). For mesoderm induction in the AB regimen, the culture medium without 5 ng/mL VEGF was used. FLK1 inhibitor, 1.2 μM ZD6474 (SelleckChem Cat. S1046) was treated from day 2 to day 3.75.

Hematopoietic and cardiac lineage induction—For hematopoietic lineage and cardiac lineage induction, mesodermal cells were sorted (see flow cytometry section) and cultured in the StemPro-34 SF medium supplemented with 2 mM Glutamax-I (ThermoFisher Scientific Cat. 35050–061), 1 mM ascorbic acid, and 30 ng/mL bFGF[24,25] for indicated duration at the density of 0.2 million cells per ml in the individual wells of a 48-well flat bottom plate (Becton Dickenson) coated with gelatin (MilliporeSigma).

Flow cytometry—For cell sorting based on PDGFRα and FLK1 expression levels, embryoid bodies under mesoderm induction in the ABV or AB regimen were harvested and dissociated at the indicated time and incubated with the PE-conjugated anti-PDGFRα antibody (ThermoFisher Scientific Cat. 12–1401-81) and the PE/Cy7-conjugated anti-FLK1 antibody (Biolegend Cat. 359911) for 1 h on ice. Cells were sorted by the PDGFRα and FLK1 staining levels into the StemPro34 medium using the FACSAria II sorting instrument

Author Manuscript Author Manuscript Author Manuscript Author Manuscript

(BD Bioscience). For cardiac troponin (cTnT) staining, Day 8 cells were harvested and fixed with cytofix/cytoperm fixation/permeabilization solution (BD Bioscience, Cat. 554714) following manufacturer's instructions. Cells were incubated with BV421-labeled anti-cTnT antibody (BD Bioscience Cat. 565618) for 1.5 h and analyzed by LSRFortessa cell analyzer (BD Bioscience). Flowjo software was used to visualize flow cytometry data.

Immunofluorescence—For immunohistochemistry, the Day 8 cells were fixed with 4% formaldehyde (ThermoFisher Scientific) for 24 h and washed with PBS. Cells were permeabilized in PBS containing 0.25% Triton X-100 for 10 min. The anti-cTnT antibody (Thermo Fisher Scientific, Cat. MS-295) and anti-myosin heavy chain class II (Abcam Cat. ab55152) antibodies were used.

Blood colony-forming assay—Twelve thousand cells were plated at 2 days after cell sorting (Day 6 post differentiation) into a methylcellulose-based medium containing hematopoietic cytokines (MethoCult M3434, StemCell Technologies, Cat. 03434). Hematopoietic colonies were counted by manufacturer's instructions at 10 days post-plating (Day 16 of differentiation).

Quantitative RT-PCR—Quantitative real-time RT-PCR was performed using an ABI Prism 7500 Fast SDS (Applied Biosystems). Total RNA was extracted using NucleoSpin RNAII kit (Takara, Cat#740955.50). qRT-PCR was performed on 96-well optical reaction plates with one-step SYBR Green PCR master mix (Bio-Rad Laboratories, Cat#1725150).

RNA-seq—Library preparation was performed by the University of Chicago Genomics Facility using the Illumina TruSeq RNA Sample prep kit v2 (Part #RS-122–2001). Library fragments were approximately 275bps in length and were quantitated using the Agilent Bio-analyzer 2100 and pooled in equimolar amounts. Single-ended, 51bp sequencing was performed on the Illumina HiSeq2500 in Rapid Run Mode by the University of Chicago Facility.

RNA-seq data preprocessing—Transcripts were aligned to the indexed reference for mm10 with default settings using TopHat2 v2.1.1.[60,61] Reads were filtered using bamtools using the following settings: -isDuplicate false -mapQuality ">10".[90] Transcript reads (TPMs) were counted post-alignment using StringTie.[62,91] TPMs are listed in Table S1. Raw and processed RNA-seq data are available at GEO with an accession number GSE136692.

Differentially expressed genes—Differential expression testing was performed using edgeR v3.16.5[63–67] and limma v3.30.13[68] packages in R v3.3.2. Low level genes were removed within each condition using median $\log_2$-transformed counts per gene per million mapped reads (cpm) of 1 and a union generated from those lists. Differential expression testing was performed using a general linear model (GLM) framework. For comparing *PF* and PF^{-VEGF}, a covariate for replicate was included to correct for batch effect. Genes with absolute $\log_2$ fold change greater than 0.5 and false discovery rate (FDR) smaller than 5% were defined as differentially expressed genes. The human TF annotation[92] was downloaded from http://humantfs.ccbr.utoronto.ca/download.php and incorporated into the mouse gene list based on the gene symbols. Differentially expressed genes are listed in Table S1.

Author Manuscript Author Manuscript Author Manuscript Author Manuscript

Clustering of genes using RNA-seq data—First, the union of differentially expressed genes in the *P*-vs-*PF* and *PF*-vs-*F* comparisons was selected. Second, for each of the union differentially expressed genes, mean TPMs (mTPM) across replicates were computed. Third, for each gene, the *Z* score of Log_{10}(1+mTPM) was computed across conditions (*P*, *PF*, and *F*). Forth, the *Z* score matrix was processed using the *kmeans* function in R with k = 6 and set.seed(109). Finally, the *Z* score matrix was processed in the *fviz_nbclust* function in the factoextra package in R to compute the total within sum of square for k = 1 to k10, which supported that the choice of k = 6 was reasonable based on the total within-sum of square approaching the minimum.

ATAC-seq—ATAC-seq (Assay for Transposase-Accessible Chromatin using sequencing) was performed as previously described.[93] Libraries were amplified and normalized with the Illumina Nextera DNA Library prep kit (FC-121–1031) according to the manufacturer's protocols. Libraries were quantitated using the Agilent Bioanalyzer, pooled in equimolar amounts, and sequenced with 50-bp single-end reads on the Illumina HiSeq following the manufacturer's protocols through the Genomics Core Facility at the University of Chicago.

ATAC-seq data preprocessing—Sequencing reads were aligned to the mm10 genome using Bowtie2 v2.3.0[69] and SAMtools v0.1.19.[70,71] Peak calling was performed using MACS2 callpeak[72,73] using the settings –nomodel –shift 100 –extsize 200 -q 0.1 after pooling biological replicates. A fold-enrichment track was generated using MACS2 using the bdgcmp function (-m FE) for visualization on the genome browser. Following removal of ENCODE blacklist sites,[94,95] a union set of sites was generated by identifying summits that overlapped within 200bp and arbitrarily selecting the summit of highest positional value. Summits were then extended by 200bp in both directions to create the set of union sites. The union set of sites utilizes biological groups not explicitly described in this manuscript, but are relevant and publicly accessible through GEO. Fold-enrichment scores were assigned to each site using the multiBigwigSummary function from deepTools.[74]

Differentially accessible sites—For differentially accessible site analysis, we first extracted ATAC sites that were identified in either of the two datasets under comparison or both. The fold-enrichment scores for this set of ATAC sites were processed using a general linear model in edgeR v3.16.5[63–67] and limma v3.30.13[68] packages in R v3.3.2 to identify differentially accessible sites. Differentially accessible sites with the p-value less than 10^{-3} and absolute log_2 fold change greater than 1 were selected for downstream analyses. The list of differentially accessible sites are listed in Table S3.

Clustering of accessible sites using ATAC-seq data—First, the union of differentially accessible sites in the *P*-vs-*PF* and *PF*-vs-*F* comparisons was selected. Second, for each of the union differentially accessible sites, the *Z* score of ATAC fold-enrichment score across conditions (*P*, *PF*, and *F*) was computed. Third, the *Z* score matrix was processed using the *kmeans* function in R with k = 5 and set.seed(109). Finally, the *Z* score matrix was processed in the *fviz_nbclust* function in the factoextra package in R to compute the total within sum of square for k = 1 to k10, which supported that the choice of k = 5 was reasonable based on the total within-sum of square approaching the minimum.

Author Manuscript Author Manuscript Author Manuscript Author Manuscript

H3K27ac ChIP-seq—Cells sorted at Day 4 or Day 5 of differentiation and frozen with liquid nitrogen were crosslinked in 0.5% formaldehyde for 5 min at room temperature, and then the reaction was quenched with 125 mM glycine. Cross-linked cells were rinsed with PBST (PBS with 0.1% Tween 20) and then resuspended in LB3-Triton (1 mM EDTA, 0.5 mM EGTA, 10 mM Tris-HCl pH 8, 100 mM NaCl, 0.1% Na-Deoxycholate, 0.5% N-lauroyl sarcosine, 1% Triton) supplemented with a protease inhibitor cocktail (Calbiochem 539131). Chromatin was extracted by sonication using Bioruptor (Diagenode). Cell extract was cleared by centrifugation and an aliquot was saved for input DNA sequencing. Cell extract from 0.5 million cells was incubated with mouse monoclonal anti-H3K27ac antibody (Wako MABI0309, Lot 14007; 2 μL per IP) in A 200 μL reaction for 12 h or longer at 4°C. Immunocomplex was captured by Protein G-conjugated magnetic dynabeads (ThermoFisher) and washed. Immunoprecipitated DNA was reverse-crosslinked and used to construct high-throughput sequencing libraries using NEBNext Ultra II DNA Library Prep Kit (New England Biolabs). DNA libraries were processed on an Illumina HiSeq machine for paired-end sequencing.

H3K27ac ChIP-seq data processing and analysis—Paired-end ChIP-seq reads were aligned to the mouse reference genome mm10 using Bowtie2 with the "–no-mixed –no-discordant -X 1000" parameter set,[69] and then aligned reads with MAPQ >20 were retained. H3K27ac-enriched peaks were identified using MACS[72] with two biological replicates of ChIP and one biological replicate of the input data, with the default narrow-peak option. An ATAC site was considered overlapping with a H3K27ac region, if the ATAC site (400 bp in size) overlaps the H3K27ac peak region by at least 1 bp, as determined by the *intersect* function of BedTools.[75] For data visualization, input-normalized per-base fold-enrichment scores were computed using MACS2 with two biological replicates of ChIP and one biological replicate of the input data. We then computed the sum of the signal coverage of the fold-enrichment data within 50-bp windows across the genome, and the 50-bp window data were quantile-normalized across all experimental conditions (Day4 $PF^{-VEGF,}$ Day4 *PF*, and Day 5 *F*) using *normalize.-quantiles* function in the preprocessCore package (v1.36.0) in software R.[76] The list of H3K27ac enriched regions are listed in Table S4.

ETV2-binding sites—We used the previously published ETV2 ChIP-seq data performed in an FLK-positive cell population derived from mESC differentiation,[41] available at GEO under the accession ID GSE59402. This dataset used a mESC cell line that carries a V5-epitope tagged ETV2 transgene under the doxycycline-inducible promoter.[41] In the experiment, the V5-epitope tagged ETV2 was expressed from Day 2 to Day 3.5 of differentiation by doxycycline, and ETV-associated chromatin was immunoprecipitated using an anti-ETV2 antibody or an anti-V5 tag antibody.[41] We aligned sequencing reads to the mm10 mouse reference genome using Bowtie2[69] with the default "–sensitive" parameter. Reads with MAPQ scores greater than 20 were used in downstream analyses. Reads from biological replicates of ChIP and the corresponding input were processed by MACS2 (v2.1.0).[72,73] Aligned reads from three ChIP-seq replicates (one replicate from anti-ETV2 ChIP and two replicates from anti-V5 ChIP; Short Read Archive IDs SRR1514692, SRR1514695, SRR1514696) and aligned reads from two control ChIP experiments (one replicate from non-ETV2 induced cells and one replicate from IgG control; Short Read

Author Manuscript Author Manuscript Author Manuscript Author Manuscript

Archive IDs SRR1514691 and SRR1514694) were used in MACS2 program[72,73] to identify statistically overrepresented peak regions and peak summits and to produce fold-enrichment scores. The parameters used in MACS2 were [call-peak -g hg –nomodel –extsize 200 –call-summits]. Identified ETV2-enriched regions with the p value $<10^{-10}$ and the fold enrichment score greater than 4 that did not overlap ENCODE mm10 blacklisted regions (https://www.encodeproject.org/annotations/ENCSR636HFF/) or the mitochondrial genome were selected. This yielded 3,868 ETV2-binding sites (Table S4). An ATAC site was considered possessing ETV2-binding sites when the 400-bp region centered around the ATAC site summit overlapped the summit of at least one ETV2-binding site.

TF footprint analysis—We used the TOBIAS package for the TF footprint analysis using ATAC-seq data.[77] First, replicate-combined ATAC-seq read data were processed by TOBIAS *ATACorrect* function to generate signal tracks corrected for the estimated Tn5 transposase sequence bias. Second, the bias-corrected data were processed by TOBIAS *ScoreBigwig* function to calculate footprint scores across the union of ATAC sites identified in *P*, *PF*, and *F*. Third, the footprint scores were processed by TOBIAS *BINDetect* function to detect footprints at ETV2 motifs within the first-wave ATAC sites or the second-wave ATAC sites with the "–motif-pvalue 0.01 –bound-pvalue 0.01" parameter set. The ETV2 motif sequence (M09067_2.00_Etv2) was acquired from the CisBP database (Database build Version 2.00) at http://cisbp.ccbr.utoronto.ca/.[96] Finally, the output files of the *BINDetect* function were processed in TOBIAS *PlotAggregate* function to generate the aggregate signal plots.

Gene ontology analysis—Gene ontology (GO) analyses were performed using Metascape.[78,79] Gene Symbols of the genes of interest were used to examine overrepresentation of Biological Process and Molecular Function GO terms with default parameters (minimum gene count 3, $p < 0.01$, enrichment over background >1.5). p-values were derived from cumulative hypergeometric statistical tests and computed in Metascape.[79] Reported GO terms in the figures are the "Summary" GO terms of all associated GO terms, and the number of genes represent the union of genes affiliated with the associated GO terms. In the network of GO terms, which was generated as a part of the Metascape analysis, all reported GO terms are shown.

DNA motif analysis—We used FIMO in the MEME suite (v5.0.5)[80] to scan for the presence of TF motifs in each ATAC site (+/−100 bp from ATAC summit). We used the Mus musculus CIS-BP TF motif database (v2.0.0),[96] which contains Position Weight Matrix and TF family annotation for each TF. For each ATAC site and for each TF, we determined whether at least one motif is present or not. We then performed, for each TF motif, Fisher's exact test with a contingency table with counts for ATAC sites with motif presence or not and differentially accessible or not. This resulted in, for each motif for each ATAC group, a p-value, odds ratio, and motif-containing fraction of ATAC sites. To find overrepresented motifs, we selected motifs with odds ratio greater than 1 and the 95% confidence interval of the odds ratio not overlapping 1. We then selected a TF motif with the highest score defined by $\log_2$(odds ratio) × fraction for each motif family. The TF name, TF family name, fraction, and the p-value are plotted in figures.

Author Manuscript Author Manuscript Author Manuscript Author Manuscript

Association between ATAC sites and genes—One ATAC site was linked to one gene when the ATAC site summit resided in the gene body or 100 kb upstream of the transcription start site (TSS) of that gene. ATAC sites that did not fulfill this condition were not linked to genes. We used the following algorithm to select a single gene when multiple genes could be linked: a) ATAC sites located in the gene body of one gene and within 100 kb upstream of another gene were assigned to the gene whose gene body contains the ATAC sites; b) ATAC sites located in the gene body of two different genes were assigned to the gene whose TSS was closer to the ATAC sites; and c) ATAC sites located within 100 kb upstream of two different genes were assigned to the gene whose TSS was closer to the ATAC sites.

Single-cell RNA-seq analysis—Single-cell RNA-seq data was downloaded from GEO (GSE130146)[46] and imported into R using Seurat package version 4.0.0.[81–84] In preprocessing, genes expressed in at least three cells were kept, and cells with less than 5% mitochondria read and greater than 2000 unique genes were kept. This preprocessing resulted in 16,249 unique genes and 2,202 cells. Genes with read counts greater than 0 were considered expressed in a cell, and genes with read counts equal to 0 were considered not expressed in a cell. To obtain expression levels, read counts were first normalized within each cell by dividing by the total counts of each cell, then multiplied by 10000, and then natural-log transformed, following the "LogNormalization" method in the Seurat package. The single-cell *P* population was defined as *pdgfra* -expressed, *Kdr*-not-expressed cells; the single-cell *PF* population was defined as *pdgfra* -expressed, *Kdr*-expressed cells; and the single-cell *F* population was defined as *Kdr*-expressed, *pdgfra*-not-expressed cells. To compute statistical significance of *Etv2*-expressed cell count differences between *P* and *PF*, Fisher's exact test examined the association between *Kdr*-expressed cells and *Etv2*-expressed cells within *pdgfra*-expressed cells. For the comparison between *PF* and *F*, Fisher's exact test examined the association between *pdgfra*-expressed cells and *Etv2*-expressed cells within *Kdr*-expressed cells. Wilcox rank-sum test examined the statistical significance of *Etv2* expression level differences between *P* and *PF* and between *PF* and *F*, using normalized read counts.

Reference genome—We used mouse reference genome mm10 for all data analyses.

Supplementary Material

Refer to Web version on PubMed Central for supplementary material.

ACKNOWLEDGMENTS

We are thankful for technical assistance from the University of Chicago Functional Genomics, Cytometry and Antibody Technology, and Light Microscopy Cores and the Cincinnati Children's Hospital Medical Center DNA Core. The graphical abstract was created with BioRender.com. This work was funded by NIH grants R01HL55337 to K.C.; R01DK119621 and P01HL146366 to B.L.B.; R21/R33AG054770 and R21HG012423 to K.I.; and R01HD111938, R01HL147571, and R01HL163523 to I.P.M. Support was also provided by NIH grants F30HL131298 to R.D.N.; F32HL156465 to J.D.S.; T32GM007183 to J.D.S. and E.H.; T32HL139430 to J.D.S.; T32HL007381 to J.D.S., C.K., R.D.N., and A.D.H.; and T32GM007197 to A.D.H. and American Heart Association 16POST30740016 for T.S.

Author Manuscript Author Manuscript Author Manuscript Author Manuscript

REFERENCES

1. Ohno S (1978). Major sex-determining genes. Monogr. Endocrinol. 11, 1–140. 10.1007/978-3-642-81261-3. [PubMed: 109750]
2. Waddington CH (2014). The Strategy of the Genes (Routledge).
3. Sulston JE, and Horvitz HR (1977). Post-embryonic cell lineages of the nematode, Caenorhabditis elegans. Dev. Biol. 56, 110–156. 10.1016/0012-1606(77)90158-0. [PubMed: 838129]
4. Stergachis AB, Neph S, Reynolds A, Humbert R, Miller B, Paige SL, Vernot B, Cheng JB, Thurman RE, Sandstrom R, et al. (2013). Developmental fate and cellular maturity encoded in human regulatory DNA landscapes. Cell 154, 888–903. 10.1016/j.cell.2013.07.020. [PubMed: 23953118]
5. Spitz F, and Furlong EEM (2012). Transcription factors: from enhancer binding to developmental control. Nat. Rev. Genet. 13, 613–626. 10.1038/nrg3207. [PubMed: 22868264]
6. Levine M, and Davidson EH (2005). Gene regulatory networks for development. Proc. Natl. Acad. Sci. USA 102, 4936–4942. 10.1073/pnas.0408031102. [PubMed: 15788537]
7. Moris N, Pina C, and Arias AM (2016). Transition states and cell fate decisions in epigenetic landscapes. Nat. Rev. Genet. 17, 693–703. 10.1038/nrg.2016.98. [PubMed: 27616569]
8. Miroshnikova YA, Shahbazi MN, Negrete J, Chalut KJ, and Smith A (2023). Cell state transitions: catch them if you can. Development 150, dev201139. 10.1242/dev.201139. [PubMed: 36930528]
9. Wagner DE, and Klein AM (2020). Lineage tracing meets single-cell omics: opportunities and challenges. Nat. Rev. Genet. 21, 410–427. 10.1038/s41576-020-0223-2. [PubMed: 32235876]
10. Buenrostro JD, Corces MR, Lareau CA, Wu B, Schep AN, Aryee MJ, Majeti R, Chang HY, and Greenleaf WJ (2018). Integrated single-cell analysis maps the continuous regulatory Landscape of human hematopoietic differentiation. Cell 173, 1535–1548.e16. 10.1016/j.cell.2018.03.074. [PubMed: 29706549]
11. Olsson A, Venkatasubramanian M, Chaudhri VK, Aronow BJ, Salomonis N, Singh H, and Grimes HL (2016). Single-cell analysis of mixed-lineage states leading to a binary cell fate choice. Nature 537, 698–702. 10.1038/nature19348. [PubMed: 27580035]
12. Velten L, Haas SF, Raffel S, Blaszkiewicz S, Islam S, Hennig BP,Hirche C, Lutz C, Buss EC, Nowak D, et al. (2017). Human haematopoietic stem cell lineage commitment is a continuous process. Nat. Cell Biol. 19, 271–281. 10.1038/ncb3493. [PubMed: 28319093]
13. Hu M, Krause D, Greaves M, Sharkis S, Dexter M, Heyworth C, and Enver T (1997). Multilineage gene expression precedes commitment in the hemopoietic system. Genes Dev. 11, 774–785. 10.1101/gad.11.6.774. [PubMed: 9087431]
14. Brunskill EW, Park J-S, Chung E, Chen F, Magella B, and Potter SS (2014). Single cell dissection of early kidney development: multiline-age priming. Development 141, 3093–3101. 10.1242/dev.110601. [PubMed: 25053437]
15. Miyamoto T, Iwasaki H, Reizis B, Ye M, GraF T, Weissman IL, and Akashi K (2002). Myeloid or lymphoid promiscuity as a critical step in hematopoietic lineage commitment. Dev. Cell 3, 137–147. 10.1016/s1534-5807(02)00201-0. [PubMed: 12110174]
16. Kontaraki J, Chen HH, Riggs A, and Bonifer C (2000). Chromatin fine structure profiles for a developmentally regulated gene: reorganization of the lysozyme locus before trans-activator binding and gene expression. Genes Dev. 14, 2106–2122. 10.1101/gad.14.16.2106. [PubMed: 10950873]
17. Choi K, Kennedy M, Kazarov A, Papadimitriou JC, and Keller G(1998). A common precursor for hematopoietic and endothelial cells. Development 125, 725–732. 10.1242/dev.125.4.725. [PubMed: 9435292]
18. Ema M, Faloon P, Zhang WJ, Hirashima M, Reid T, Stanford WL, Orkin S, Choi K, and Rossant J (2003). Combinatorial effects of Flk1 and Tal1 on vascular and hematopoietic development in the mouse. Genes Dev. 17, 380–393. 10.1101/gad.1049803. [PubMed: 12569129]
19. Kataoka H, Takakura N, Nishikawa S, Tsuchida K, Kodama H, Kunisada T, Risau W, Kita T, and Nishikawa S-I (1997). Expressions of PDGF receptor alpha, c-Kit and Flk1 genes clustering in mouse chromosome 5 define distinct subsets of nascent mesodermal cells. Dev. Growth Differ. 39, 729–740. 10.1046/j.1440-169x.1997.t01-5-00009.x. [PubMed: 9493833]

Author Manuscript Author Manuscript Author Manuscript Author Manuscript

20. Park C, Afrikanova I, Chung YS, Zhang WJ, Arentson E, Fong Gh G.h., Rosendahl A, and Choi K (2004). A hierarchical order of factors in the generation of FLK1- and SCL-expressing hematopoietic and endothelial progenitors from embryonic stem cells. Development 131, 2749–2762. 10.1242/dev.01130. [PubMed: 15148304]
21. Shalaby F, Rossant J, Yamaguchi TP, Gertsenstein M, Wu XF, Breitman ML, and Schuh AC (1995). Failure of blood-island formation and vasculogenesis in Flk-1-deficient mice. Nature 376, 62–66. 10.1038/376062a0. [PubMed: 7596435]
22. Shalaby F, Ho J, Stanford WL, Fischer KD, Schuh AC, Schwartz L, Bernstein A, and Rossant J (1997). A requirement for Flk1 in primitive and definitive hematopoiesis and vasculogenesis. Cell 89, 981–990. 10.1016/s0092-8674(00)80283-4. [PubMed: 9200616]
23. Yamashita J, Itoh H, Hirashima M, Ogawa M, Nishikawa S, Yurugi T, Naito M, Nakao K, and Nishikawa S (2000). Flk1-positive cells derived from embryonic stem cells serve as vascular progenitors. Nature 408, 92–96. 10.1038/35040568. [PubMed: 11081514]
24. Kattman SJ, Huber TL, and Keller GM (2006). Multipotent flk-1+ cardiovascular progenitor cells give rise to the cardiomyocyte, endothelial, and vascular smooth muscle lineages. Dev. Cell 11, 723–732. 10.1016/j.devcel.2006.10.002. [PubMed: 17084363]
25. Kattman SJ, Witty AD, Gagliardi M, Dubois NC, Niapour M, Hotta A, Ellis J, and Keller G (2011). Stage-specific optimization of activin/nodal and BMP signaling promotes cardiac differentiation of mouse and human pluripotent stem cell lines. Cell Stem Cell 8, 228–240. 10.1016/j.stem.2010.12.008. [PubMed: 21295278]
26. Moretti A, Caron L, Nakano A, Lam JT, Bernshausen A, Chen Y, Qyang Y, Bu L, Sasaki M, Martin-Puig S, et al. (2006). Multipotent embryonic isl1+ progenitor cells lead to cardiac, smooth muscle, and endothelial cell diversification. Cell 127, 1151–1165. 10.1016/j.cell.2006.10.029. [PubMed: 17123592]
27. Motoike T, Markham DW, Rossant J, and Sato TN (2003). Evidence for novel fate of Flk1+ progenitor: contribution to muscle lineage. Genesis 35, 153–159. 10.1002/gene.10175. [PubMed: 12640619]
28. Yang L, Soonpaa MH, Adler ED, Roepke TK, Kattman SJ, Kennedy M, Henckaerts E, Bonham K, Abbott GW, Linden RM, et al. (2008). Human cardiovascular progenitor cells develop from a KDR+ embryonic-stem-cell-derived population. Nature 453, 524–528. 10.1038/nature06894. [PubMed: 18432194]
29. Kataoka H, Hayashi M, Nakagawa R, Tanaka Y, Izumi N, Nishikawa S, Jakt ML, Tarui H, and Nishikawa S-I (2011). Etv2/ER71 induces vascular mesoderm from Flk1+PDGFRα+ primitive mesoderm. Blood 118, 6975–6986. 10.1182/blood-2011-05-352658. [PubMed: 21911838]
30. Rasmussen TL, Shi X, Wallis A, Kweon J, Zirbes KM, Koyano-Nakagawa N, and Garry DJ (2012). VEGF/Flk1 signaling cascade transactivates Etv2 gene expression. PLoS One 7, e50103. 10.1371/journal.pone.0050103. [PubMed: 23185546]
31. Zhao H, and Choi K (2017). A CRISPR screen identifies genes controlling Etv2 threshold expression in murine hemangiogenic fate commitment. Nat. Commun. 8, 541. 10.1038/s41467-017-00667-5. [PubMed: 28912455]
32. Lee D, Park C, Lee H, Lugus JJ, Kim SH, Arentson E, Chung YS, Gomez G, Kyba M, Lin S, et al. (2008). ER71 acts downstream of BMP, Notch, and Wnt signaling in blood and vessel progenitor specification. Cell Stem Cell 2, 497–507. 10.1016/j.stem.2008.03.008. [PubMed: 18462699]
33. Wareing S, Mazan A, Pearson S, Göttgens B, Lacaud G, and Kouskoff V (2012). The Flk1-Cre-mediated deletion of ETV2 defines its narrow temporal requirement during embryonic hematopoietic development. Stem Cell. 30, 1521–1531. 10.1002/stem.1115.
34. Elcheva I, Brok-Volchanskaya V, Kumar A, Liu P, Lee J-H, Tong L, Vodyanik M, Swanson S, Stewart R, Kyba M, et al. (2014). Direct induction of haematoendothelial programs in human pluripotent stem cells by transcriptional regulators. Nat. Commun. 5, 4372. 10.1038/ncomms5372. [PubMed: 25019369]
35. De Val S, Chi NC, Meadows SM, Minovitsky S, Anderson JP, Harris IS, Ehlers ML, Agarwal P, Visel A, Xu S-M, et al. (2008). Combinatorial regulation of endothelial gene expression by ets and forkhead transcription factors. Cell 135, 1053–1064. 10.1016/j.cell.10.049. [PubMed: 19070576]

Author Manuscript Author Manuscript Author Manuscript Author Manuscript

36. Ferdous A, Caprioli A, Iacovino M, Martin CM, Morris J, Richardson JA, Latif S, Hammer RE, Harvey RP, Olson EN, et al. (2009). Nkx2–5 transactivates the Ets-related protein 71 gene and specifies an endothelial/endocardial fate in the developing embryo. Proc. Natl. Acad. Sci. USA 106, 814–819. 10.1073/pnas.0807583106. [PubMed: 19129488]
37. Morita R, Suzuki M, Kasahara H, Shimizu N, Shichita T, Sekiya T, Kimura A, Sasaki K-I, Yasukawa H, and Yoshimura A (2015). ETS transcription factor ETV2 directly converts human fibroblasts into functional endothelial cells. Proc. Natl. Acad. Sci. USA 112, 160–165. 10.1073/pnas.1413234112. [PubMed: 25540418]
38. Veldman MB, Zhao C, Gomez GA, Lindgren AG, Huang H, Yang H, Yao S, Martin BL, Kimelman D, and Lin S (2013). Transdifferentiation of fast skeletal muscle into functional endothelium *in vivo* by transcription factor Etv2. PLoS Biol. 11, e1001590. 10.1371/journal.pbio.1001590. [PubMed: 23853546]
39. De Val S, and Black BL (2009). Transcriptional control of endothelial cell development. Dev. Cell 16, 180–195. 10.1016/j.devcel.01.014. [PubMed: 19217421]
40. Koyano-Nakagawa N, and Garry DJ (2017). Etv2 as an essential regulator of mesodermal lineage development. Cardiovasc. Res. 113, 1294–1306. 10.1093/cvr/cvx133. [PubMed: 28859300]
41. Liu F, Li D, Yu YYL, Kang I, Cha M-J, Kim JY, Park C, Watson DK, Wang T, and Choi K (2015). Induction of hematopoietic and endothelial cell program orchestrated by ETS transcription factor ER71/ETV2. EMBO Rep. 16, 654–669. 10.15252/embr.201439939. [PubMed: 25802403]
42. Palencia-Desai S, Kohli V, Kang J, Chi NC, Black BL, and Sumanas S (2011). Vascular endothelial and endocardial progenitors differentiate as cardiomyocytes in the absence of Etsrp/Etv2 function. Development 138, 4721–4732. 10.1242/dev.064998. [PubMed: 21989916]
43. Rasmussen TL, Kweon J, Diekmann MA, Belema-Bedada F, Song Q, Bowlin K, Shi X, Ferdous A, Li T, Kyba M, et al. (2011). ER71 directs mesodermal fate decisions during embryogenesis. Development 138, 4801–4812. 10.1242/dev.070912. [PubMed: 21989919]
44. Stennard FA, and Harvey RP (2005). T-box transcription factors and their roles in regulatory hierarchies in the developing heart. Development 132, 4897–4910. 10.1242/dev.02099. [PubMed: 16258075]
45. Tremblay M, Sanchez-Ferras O, and Bouchard M (2018). GATA transcription factors in development and disease. Development 145, dev164384. 10.1242/dev.164384. [PubMed: 30348673]
46. Zhao H, and Choi K (2019). Single cell transcriptome dynamics from pluripotency to FLK1 mesoderm. Development 146, dev182097. 10.1242/dev.182097. [PubMed: 31740535]
47. Zaret K (1997). Identifying specific protein-DNA interactions within living cells, or in “in vivo footprinting. Methods 11, 149–150. 10.1006/meth.1996.0400. [PubMed: 8993026]
48. Neph S, Vierstra J, Stergachis AB, Reynolds AP, Haugen E, Vernot B, Thurman RE, John S, Sandstrom R, Johnson AK, et al. (2012). An expansive human regulatory lexicon encoded in transcription factor footprints. Nature 489, 83–90. 10.1038/nature11212. [PubMed: 22955618]
49. Lilly AJ, Mazan A, Scott DA, Lacaud G, and Kouskoff V (2017). SOX7 expression is critically required in FLK1-expressing cells for vasculogenesis and angiogenesis during mouse embryonic development. Mech. Dev. 146, 31–41. 10.1016/j.mod.2017.05.004. [PubMed: 28577909]
50. Behrens AN, Zierold C, Shi X, Ren Y, Koyano-Nakagawa N, Garry DJ, and Martin CM (2014). Sox7 is regulated by ETV2 during cardiovascular development. Stem Cells Dev. 23, 2004–2013. 10.1089/scd.2013.0525. [PubMed: 24762086]
51. Sinha T, Lammerts van Bueren K, Dickel DE, Zlatanova I, Thomas R, Lizama CO, Xu S-M, Zovein AC, Ikegami K, Moskowitz IP, et al. (2022). Differential Etv2 threshold requirement for endothelial and erythropoietic development. Cell Rep. 39, 110881. 10.1016/j.celrep.2022.110881. [PubMed: 35649376]
52. Lammerts van Bueren K, and Black BL (2012). Regulation of endothelial and hematopoietic development by the ETS transcription factor Etv2. Curr. Opin. Hematol 19, 199–205. 10.1097/MOH.0b013e3283523e07. [PubMed: 22406820]
53. Zhao H, Xu C, Lee T-J, Liu F, and Choi K (2017). ETS transcription factor ETV2/ER71/Etsrp in hematopoietic and vascular development, injury, and regeneration. Dev. Dyn. 246, 318–327. 10.1002/dvdy.24483. [PubMed: 28026128]

Author Manuscript Author Manuscript Author Manuscript Author Manuscript

54. Gong W, Das S, Sierra-Pagan JE, Skie E, Dsouza N, Larson TA, Garry MG, Luzete-Monteiro E, Zaret KS, and Garry DJ (2022). ETV2 functions as a pioneer factor to regulate and reprogram the endothelial lineage. Nat. Cell Biol. 24, 672–684. 10.1038/s41556-022-00901-3. [PubMed: 35550615]
55. Koyano-Nakagawa N, Shi X, Rasmussen TL, Das S, Walter CA, and Garry DJ (2015). Feedback mechanisms regulate ets variant 2 (Etv2) gene expression and hematoendothelial lineages. J. Biol. Chem. 290, 28107–28119. 10.1074/jbc.M115.662197. [PubMed: 26396195]
56. Paige SL, Thomas S, Stoick-Cooper CL, Wang H, Maves L, Sandstrom R, Pabon L, Reinecke H, Pratt G, Keller G, et al. (2012). A temporal chromatin signature in human embryonic stem cells identifies regulators of cardiac development. Cell 151, 221–232. 10.1016/j.cell.2012.08.027. [PubMed: 22981225]
57. Bendall SC, Davis KL, Amir E-AD, Tadmor MD, Simonds EF, Chen TJ, Shenfeld DK, Nolan GP, and Pe'er D (2014). Single-cell trajectory detection uncovers progression and regulatory coordination in human B cell development. Cell 157, 714–725. 10.1016/j.cell.2014.04.005. [PubMed: 24766814]
58. Trapnell C, Cacchiarelli D, Grimsby J, Pokharel P, Li S, Morse M, Lennon NJ, Livak KJ, Mikkelsen TS, and Rinn JL (2014). The dynamics and regulators of cell fate decisions are revealed by pseudotemporal ordering of single cells. Nat. Biotechnol. 32, 381–386. 10.1038/nbt.2859. [PubMed: 24658644]
59. Ma S, Zhang B, LaFave LM, Earl AS, Chiang Z, Hu Y, Ding J, Brack A, Kartha VK, Tay T, et al. (2020). Chromatin potential identified by shared single-cell profiling of RNA and chromatin. Cell 183, 1103–1116.e20. 10.1016/j.cell.2020.09.056. [PubMed: 33098772]
60. Trapnell C, Pachter L, and Salzberg SL (2009). TopHat: discovering splice junctions with RNA-Seq. Bioinformatics 25, 1105–1111. 10.1093/bioinformatics/btp120. [PubMed: 19289445]
61. Kim D, Pertea G, Trapnell C, Pimentel H, Kelley R, and Salzberg SL (2013). TopHat2: accurate alignment of transcriptomes in the presence of insertions, deletions and gene fusions. Genome Biol. 14, R36. 10.1186/gb-2013-14-4-r36. [PubMed: 23618408]
62. Pertea M, Kim D, Pertea GM, Leek JT, and Salzberg SL (2016). Transcript-level expression analysis of RNA-seq experiments with HISAT, StringTie and Ballgown. Nat. Protoc. 11, 1650–1667. 10.1038/nprot.2016.095. [PubMed: 27560171]
63. McCarthy DJ, Chen Y, and Smyth GK (2012). Differential expression analysis of multifactor RNA-Seq experiments with respect to biological variation. Nucleic Acids Res. 40, 4288–4297. 10.1093/nar/gks042. [PubMed: 22287627]
64. Robinson MD, and Smyth GK (2007). Moderated statistical tests for assessing differences in tag abundance. Bioinformatics 23, 2881–2887. 10.1093/bioinformatics/btm453. [PubMed: 17881408]
65. Robinson MD, and Smyth GK (2008). Small-sample estimation of negative binomial dispersion, with applications to SAGE data. Biostatistics 9, 321–332. 10.1093/biostatistics/kxm030. [PubMed: 17728317]
66. Robinson MD, McCarthy DJ, and Smyth GK (2010). edgeR: a Bioconductor package for differential expression analysis of digital gene expression data. Bioinformatics 26, 139–140. 10.1093/bioinformatics/btp616. [PubMed: 19910308]
67. Zhou X, Lindsay H, and Robinson MD (2014). Robustly detecting differential expression in RNA sequencing data using observation weights. Nucleic Acids Res. 42, e91. 10.1093/nar/gku310. [PubMed: 24753412]
68. Ritchie ME, Phipson B, Wu D, Hu Y, Law CW, Shi W, and Smyth GK (2015). Limma powers differential expression analyses for RNA-sequencing and microarray studies. Nucleic Acids Res. 43, e47. 10.1093/nar/gkv007. [PubMed: 25605792]
69. Langmead B, and Salzberg SL (2012). Fast gapped-read alignment with Bowtie 2. Nat. Methods 9, 357–359. 10.1038/nmeth.1923. [PubMed: 22388286]
70. Li H, Handsaker B, Wysoker A, Fennell T, Ruan J, Homer N, Marth G, Abecasis G, and Durbin R; 1000 Genome Project Data Processing Subgroup (2009). The sequence alignment/map format and SAMtools. Bioinformatics 25, 2078–2079. 10.1093/bioinformatics/btp352. [PubMed: 19505943]

Author Manuscript Author Manuscript Author Manuscript Author Manuscript

71. Li H (2011). A statistical framework for SNP calling, mutation discovery, association mapping and population genetical parameter estimation from sequencing data. Bioinformatics 27, 2987–2993. 10.1093/bioinformatics/btr509. [PubMed: 21903627]
72. Feng J, Liu T, Qin B, Zhang Y, and Liu XS (2012). Identifying ChIP-seq enrichment using MACS. Nat. Protoc. 7, 1728–1740. 10.1038/nprot.2012.101. [PubMed: 22936215]
73. Zhang Y, Liu T, Meyer CA, Eeckhoute J, Johnson DS, Bernstein BE, Nusbaum C, Myers RM, Brown M, Li W, and Liu XS (2008). Model-based analysis of ChIP-seq (MACS). Genome Biol. 9, R137. 10.1186/gb-2008-9-9-r137. [PubMed: 18798982]
74. Ramírez F, Ryan DP, Grüning B, Bhardwaj V, Kilpert F, Richter AS, Heyne S, Dündar F, and Manke T (2016). deepTools2: a next generation web server for deep-sequencing data analysis. Nucleic Acids Res. 44, W160–W165. 10.1093/nar/gkw257. [PubMed: 27079975]
75. Quinlan AR, and Hall IM (2010). BEDTools: a flexible suite of utilities for comparing genomic features. Bioinformatics 26, 841–842. 10.1093/bioinformatics/btq033. [PubMed: 20110278]
76. Bolstad BM, Irizarry RA, Astrand M, and Speed TP (2003). A comparison of normalization methods for high density oligonucleotide array data based on variance and bias. Bioinformatics 19, 185–193. 10.1093/bioinformatics/19.2.185. [PubMed: 12538238]
77. Bentsen M, Goymann P, Schultheis H, Klee K, Petrova A, Wiegandt R, Fust A, Preussner J, Kuenne C, Braun T, et al. (2020). ATAC-seq footprinting unravels kinetics of transcription factor binding during zygotic genome activation. Nat. Commun. 11, 4267. 10.1038/s41467-020-18035-1. [PubMed: 32848148]
78. Tripathi S, Pohl MO, Zhou Y, Rodriguez-Frandsen A, Wang G, Stein DA, Moulton HM, DeJesus P, Che J, Mulder LCF, et al. (2015). Meta- and orthogonal integration of influenza "OMICs" data defines a role for UBR4 in virus budding. Cell Host Microbe 18, 723–735. 10.1016/j.chom.2015.11.002. [PubMed: 26651948]
79. Zhou Y, Zhou B, Pache L, Chang M, Khodabakhshi AH, Tanaseichuk O, Benner C, and Chanda SK (2019). Metascape provides a biologist-oriented resource for the analysis of systems-level datasets. Nat. Commun. 10, 1523. 10.1038/s41467-019-09234-6. [PubMed: 30944313]
80. Grant CE, Bailey TL, and Noble WS (2011). FIMO: scanning for occurrences of a given motif. Bioinformatics 27, 1017–1018. 10.1093/bioinformatics/btr064. [PubMed: 21330290]
81. Satija R, Farrell JA, Gennert D, Schier AF, and Regev A (2015). Spatial reconstruction of single-cell gene expression data. Nat. Biotechnol. 33, 495–502. 10.1038/nbt.3192. [PubMed: 25867923]
82. Butler A, Hoffman P, Smibert P, Papalexi E, and Satija R (2018). Integrating single-cell transcriptomic data across different conditions, technologies, and species. Nat. Biotechnol. 36, 411–420. 10.1038/nbt.4096. [PubMed: 29608179]
83. Stuart T, Butler A, Hoffman P, Hafemeister C, Papalexi E, Mauck WM 3rd, Hao Y, Stoeckius M, Smibert P, and Satija R (2019). Comprehensive integration of single-cell data. Cell 177, 1888–1902.e21. 10.1016/j.cell.2019.05.031. [PubMed: 31178118]
84. Hao Y, Hao S, Andersen-Nissen E, Mauck WM 3rd, Zheng S, Butler A, Lee MJ, Wilk AJ, Darby C, Zager M, et al. (2021). Integrated analysis of multimodal single-cell data. Cell 184, 3573–3587.e29. 10.1016/j.cell.2021.04.048. [PubMed: 34062119]
85. Iacovino M, Bosnakovski D, Fey H, Rux D, Bajwa G, Mahen E, Mitanoska A, Xu Z, and Kyba M (2011). Inducible cassette exchange: a rapid and efficient system enabling conditional gene expression in embryonic stem and primary cells. Stem Cell. 29, 1580–1588. 10.1002/stem.715.
86. Fehling HJ, Lacaud G, Kubo A, Kennedy M, Robertson S, Keller G, and Kouskoff V (2003). Tracking mesoderm induction and its specification to the hemangioblast during embryonic stem cell differentiation. Development 130, 4217–4227. 10.1242/dev.00589. [PubMed: 12874139]
87. Ying Q-L, Nichols J, Chambers I, and Smith A (2003). BMP induction of Id proteins suppresses differentiation and sustains embryonic stem cell self-renewal in collaboration with STAT3. Cell 115, 281–292. 10.1016/s0092-8674(03)00847-x. [PubMed: 14636556]
88. Ying Q-L, Wray J, Nichols J, Batlle-Morera L, Doble B, Woodgett J, Cohen P, and Smith A (2008). The ground state of embryonic stem cell self-renewal. Nature 453, 519–523. 10.1038/nature06968. [PubMed: 18497825]

Author Manuscript Author Manuscript Author Manuscript Author Manuscript

89. Gadue P, Huber TL, Paddison PJ, and Keller GM (2006). Wnt and TGF-β signaling are required for the induction of an in vitro model of primitive streak formation using embryonic stem cells. Proc. Natl. Acad. Sci. USA 103, 16806–16811. 10.1073/pnas.0603916103. [PubMed: 17077151]

90. Barnett DW, Garrison EK, Quinlan AR, Strömberg MP, and Marth GT (2011). BamTools: a C++ API and toolkit for analyzing and managing BAM files. Bioinformatics 27, 1691–1692. 10.1093/bioinformatics/btr174. [PubMed: 21493652]

91. Pertea M, Pertea GM, Antonescu CM, Chang T-C, Mendell JT, and Salzberg SL (2015). StringTie enables improved reconstruction of a transcriptome from RNA-seq reads. Nat. Biotechnol. 33, 290–295. 10.1038/nbt.3122. [PubMed: 25690850]

92. Lambert SA, Jolma A, Campitelli LF, Das PK, Yin Y, Albu M, Chen X, Taipale J, Hughes TR, and Weirauch MT (2018). The human transcription factors. Cell 175, 598–599. 10.1016/j.cell.2018.09.045. [PubMed: 30290144]

93. Buenrostro JD, Giresi PG, Zaba LC, Chang HY, and Greenleaf WJ (2013). Transposition of native chromatin for fast and sensitive epigenomic profiling of open chromatin, DNA-binding proteins and nucleosome position. Nat. Methods 10, 1213–1218. 10.1038/nmeth.2688. [PubMed: 24097267]

94. Amemiya HM, Kundaje A, and Boyle AP (2019). The ENCODE blacklist: identification of problematic regions of the genome. Sci. Rep. 9, 9354. 10.1038/s41598-019-45839-z. [PubMed: 31249361]

95. ENCODE Project Consortium (2012). An integrated encyclopedia of DNA elements in the human genome. Nature 489, 57–74. 10.1038/nature11247. [PubMed: 22955616]

96. Weirauch MT, Yang A, Albu M, Cote AG, Montenegro-Montero A, Drewe P, Najafabadi HS, Lambert SA, Mann I, Cook K, et al. (2014). Determination and inference of eukaryotic transcription factor sequence specificity. Cell 158, 1431–1443. 10.1016/j.cell.2014.08.009. [PubMed: 25215497]

Author Manuscript Author Manuscript Author Manuscript Author Manuscript

Highlights

- Accessible ETV2-binding sites emerge in multipotent progenitors prior to commitment
- Almost no ETV2-binding sites are activated until hematoendothelial fate commitment
- Second set of ETV2-binding sites are activated in committed hematoendothelial cells
- ETV2 binding to binding-site activation drives hematoendothelial commitment

Author Manuscript Author Manuscript Author Manuscript Author Manuscript

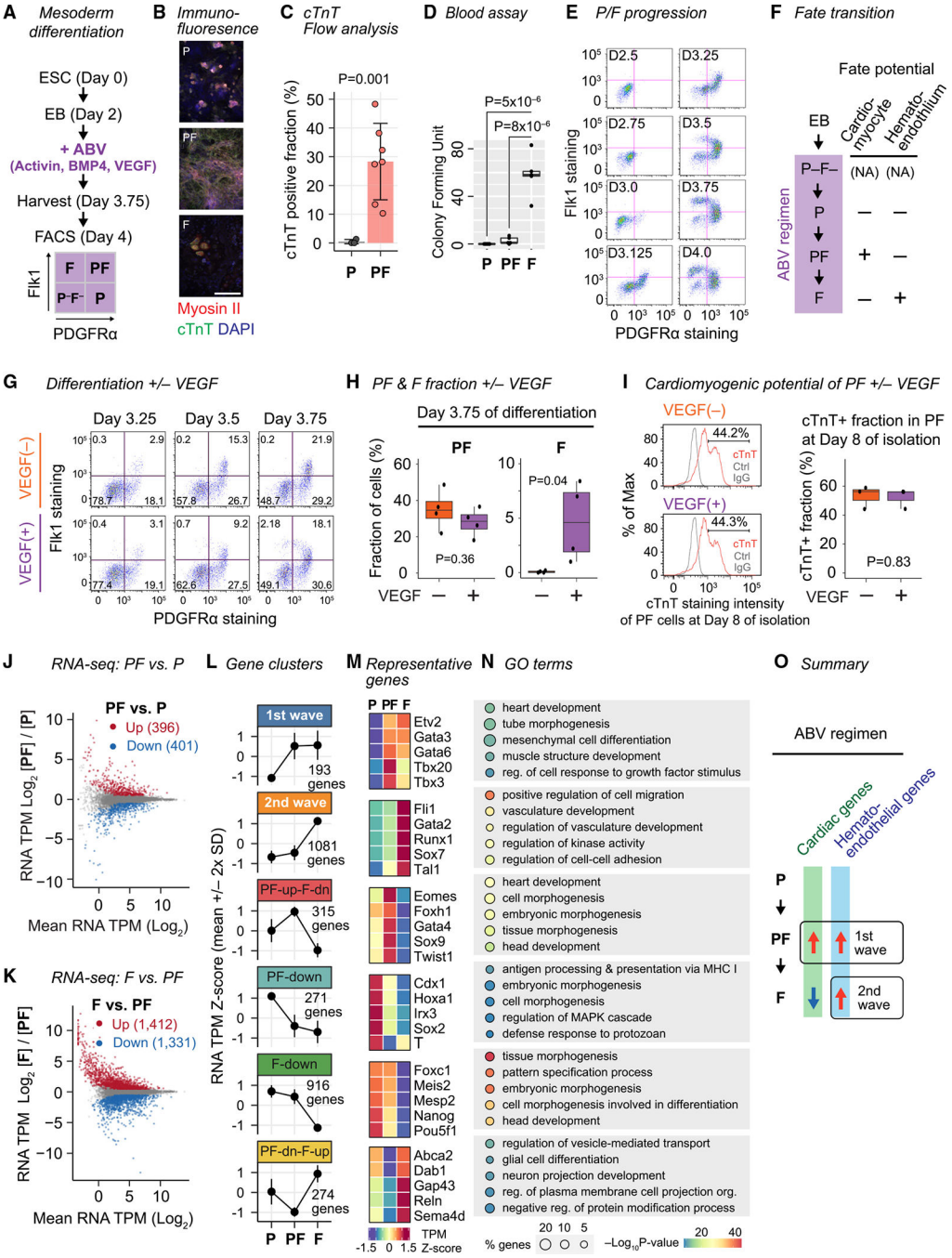

Figure 1. Two waves of hematoendothelial gene expression

(A) mESC differentiation in the ABV regimen and isolation of PDGFRα (*P*)/Flk1 (*F*) populations. See Figure S1 for additional characterization.

(B) Immunofluorescence for cardiac myosin II and cardiac troponin (cTnT) in day 4 *P*, *PF*, and *F* cells. All images same magnification; scale bar: 100 μm.

(C) Fraction of cTnT^{+} cells in day 8 *P* (n = 3) or *PF* (n = 6) cells by flow cytometry. p, generalized linear model (GLM) *P* value accounting for experiment batches. Data, mean ± SD.

Author Manuscript Author Manuscript Author Manuscript Author Manuscript

(D) Blood colony-forming units from 12,000 *P*, *PF*, or *F* cells 10 days after isolation. Data are represented by boxplot.

(E) *P/F* flow cytometry analysis at the indicated time.

(F) Temporal relationship and fate potential of *P/F* populations at day 4.

(G) *P/F* flow cytometry at the indicated time with or without VEG*F*.

(H) Fraction of *PF* and *F* populations at day 3.75 with or without VEG*F*. p, GLM *P* value accounting for treatment series batches. n = 4. Data are represented by boxplot.

(I) Flow cytometry plot (left) and quantification (right) for cTnT-stained *PF* cells at day 8. p, GLM *P* value. n = 3. Data are represented by boxplot.

(J) Transcriptome comparison between *P* and *PF* at day 4.

(K) Transcriptome comparison between *PF* and *F* at day 4.

(L) The unions of differentially expressed dynamic genes identified in (J) and (K) are clustered into 6 groups.

(M) mRNA levels of representative genes in each group from (L).

(N) Top 5 Gene Ontology (GO) terms by *P* value overrepresented in each group from (L).

(O) Two waves of gene expression toward hematoendothelial fate commitment in *F*.

Author Manuscript Author Manuscript Author Manuscript Author Manuscript

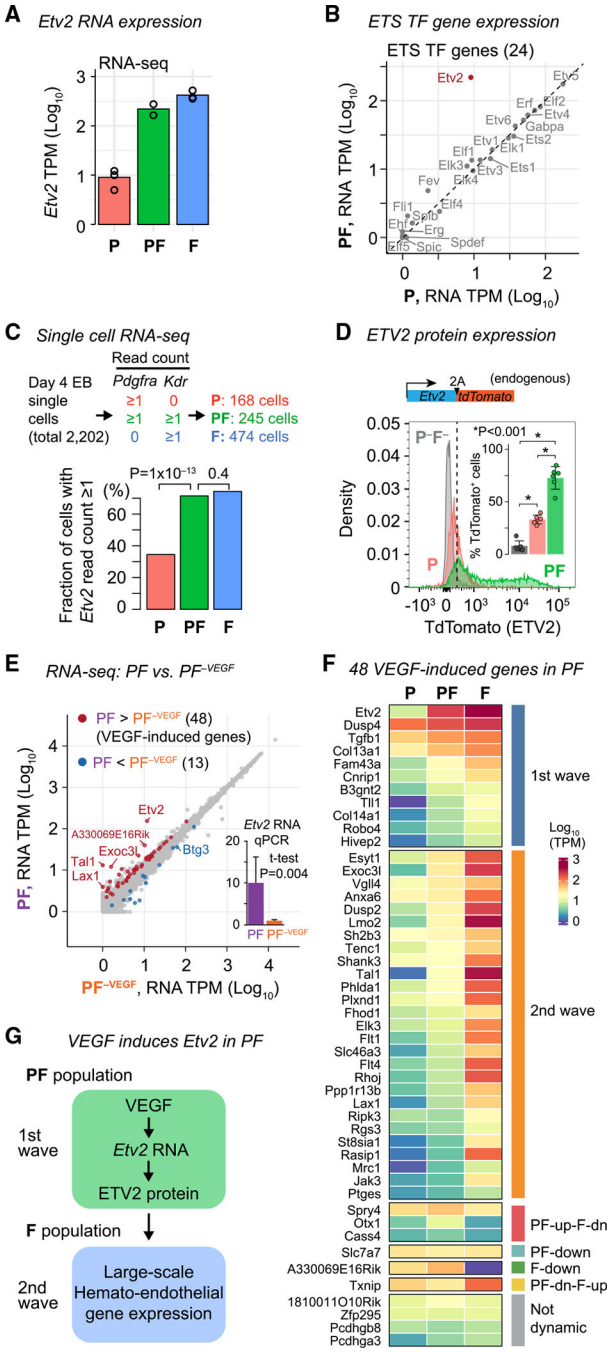

Figure 2. VEGF induces *Etv2* without inducing second-wave genes in *PF*

(A) *Etv2* mRNA levels in *P*, *PF*, and *F*. See Figure S2 for additional characterization. Data, mean with all replicates shown.

(B) Transcripts per million (TPMs) for all 24 ETS-family genes in *P* and *PF*.

(C) (Top) Cells from single-cell RNA-seq data[46] are grouped in *P*, *PF*, and *F* by *pdgfra* and *Flk1* counts. (Bottom) Fraction of *P*, *PF*, or *F* single cells expressing *Etv2*. p, Fisher's exact test p value.

Author Manuscript Author Manuscript Author Manuscript Author Manuscript

(D) Histogram of tdTomato expression levels of *P*–*F*–, *P*, and *PF* cells at day 4 of differentiation of ETV2–2A-tdTomato transgenic mESC. (Inset) Quantification of tdTomato^{+} cells. p, GLM p value accounting for experiment batches. Data, mean ± SD.

(E) Transcriptome comparison between day 4 *PF* derived with VEGF (*PF*) and *PF* without VEGF (PF^{-VEGF}). Inset, quantitative RT-PCR for *Etv2*. p, t test p value. Data, mean ± SD.

(F) mRNA levels for the 48 VEGF-induced genes in *P*, *PF*, and *F* with VEG*F*. Genes grouped by dynamic clusters (Figure 1L).

(G) VEGF induces the first-wave gene *Etv2* without causing large-scale second-wave hematoendothelial gene expression in *PF*; second-wave expression occurs in *F*.

Author Manuscript Author Manuscript Author Manuscript Author Manuscript

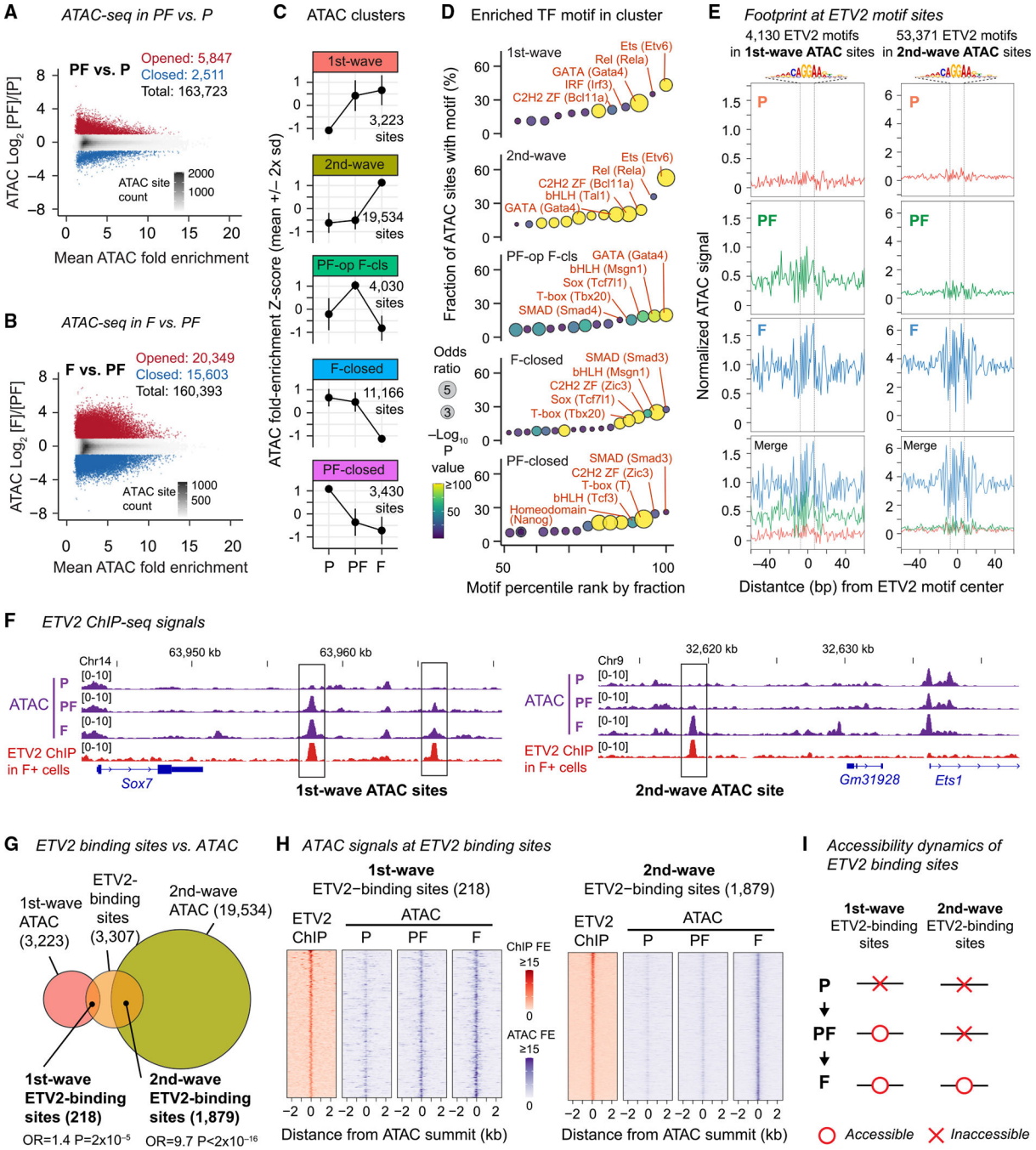

Figure 3. Accessible ETV2-binding sites emerge in *PF* and expand in *F*

(A) MA plot comparing ATAC-seq signals in *PF* vs. *P*. See Figure S3 for additional characterization.

(B) Same as (A) but shown for *F* vs. *PF*.

(C) The unions of differentially accessible sites identified in (A) and (B) are clustered into 5 groups. *PF*-opened (*PF*-op); *F*-closed (*F*-cls) sites.

(D) TF family motifs overrepresented (odds ratio >1) within clusters. Parentheses, most overrepresented TF within family.

Author Manuscript Author Manuscript Author Manuscript Author Manuscript

(E) Mean base-resolution profile of 120 bp centered around ETV2 motif center in first-wave (left) or second-wave (right) ATAC sites.

(F) ATAC and ETV2 ChIP-seq fold enrichment signal tracks showing first-wave (left) and second-wave (right) ETV2-binding sites. ETV2 ChIP-seq data are from$FLK1^+$ cells.[41]

(G) ETV2-binding sites overlapping the first-wave and second-wave ATAC sites. p, Fisher's exact test p value.

(H) ATAC-seq fold enrichment signals at first-wave (left) and second-wave (right) ETV2-binding sites.

(I) The first-wave and second-wave ETV2-binding sites differ in the timing of accessibility gains at *PF* or *F*.

Author Manuscript Author Manuscript Author Manuscript Author Manuscript

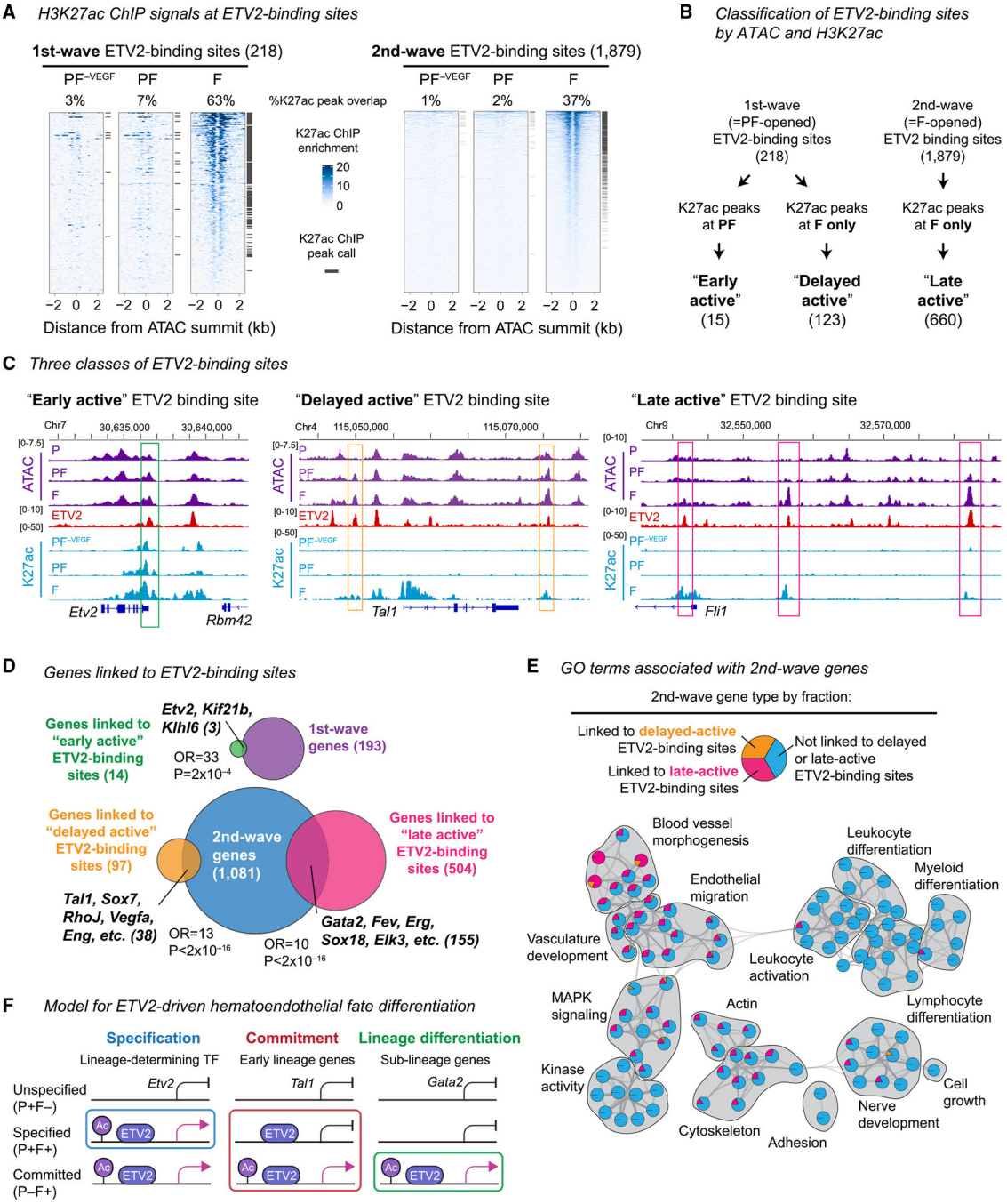

Figure 4. *PF*-opened ETV2-binding sites become activated in *F* and accompany transcriptional activation of early hematoendothelial regulators

(A) H3K27ac ChIP-seq fold enrichment signals at first-wave (left) and second-wave (right) ETV2-binding sites. H3K27ac ChIP-seq is performed in PF^{-VEGF} and *PF* isolated at day 4 and *F* isolated at Day 5. See Figure S4 for additional characterization.

(B) Classification of the first- and second-wave ETV2-binding sites into early-active, delayed-active, and late-active ETV2-binding sites.

(C) H3K27ac ChIP-seq fold enrichment signal tracks, along with ATAC-seq and ETV2 ChIP-seq tracks.

Author Manuscript Author Manuscript Author Manuscript Author Manuscript

(D) (Top) Relationship between genes linked to early-active ETV2-binding sites and the first-wave genes. (Bottom) Relationship between genes linked to delayed-active or genes linked to late-active ETV2-binding sites and the second-wave genes. Parentheses, number of genes. p, Fisher's exact test p value.

(E) GO terms overrepresented in the second-wave genes. For each GO term (circle), the fraction of the GO-associated genes linked to delayed-active (yellow) or late-active (magenta) ETV2-binding sites or not linked to delayed or late-active ETV2-binding sites (blue) are shown as a pie chart. Lines link GO terms by similarity.

(F) Timing of ETV2 binding and the timing of ETV2-bound enhancer activation distinguish different phases of hematoendothelial gene expression.

Author Manuscript Author Manuscript Author Manuscript Author Manuscript

KEY RESOURCES TABLE

REAGENT or RESOURCE	SOURCE	IDENTIFIER
Antibodies		
PE-conjugated anti-PDGFRα antibody	ThermoFisher Scientific	Cat# 12–1401-81; RRID:AB_657615
PE/Cy7-conjugated anti-Flk1 antibody	Biolegend	Cat# 359911; RRID:AB_2563551
BV421-labeled anti-cTnT antibody	BD Bioscience	Cat# 565618; AB_2739306
anti-cTnT antibody	Thermo Fisher Scientific	Cat#MS-295; RRID:AB_61810
anti-myosin heavy chain class II	Abcam	Cat#ab55152; RRID:AB_944199
anti-H3K27ac antibody	Wako	Cat#MABI0309; RRID:AB_11126964
Chemicals, peptides, and recombinant proteins		
Penicillin-streptomycin	ThermoFisher Scientific	Cat#15140148
Mono-thioglycerol	ThermoFisher Scientific	Cat#M6145
N-2 supplement	ThermoFisher Scientific	Cat#17502048
B27 supplement	ThermoFisher Scientific	Cat# 17504044
L-Glutamine	ThermoFisher Scientific	Cat# A2916801
Glutamax-I	ThermoFisher Scientific	Cat# 35050–061
Paraformaldehyde Solution	ThermoFisher Scientific	Cat# J19943.K2
Triton X-100	ThermoFisher Scientific	Cat#A16046-AE
Neurobasal medium	ThermoFisher Scientific	Cat# 21103049
DMEM/F12 medium	ThermoFisher Scientific	Cat# 10565018
Iscove's modified Dubelcco's medium (IMDM)	ThermoFisher Scientific	Cat# 31980030
Ham's F12 medium	ThermoFisher Scientific	Cat# 31765035
Stempro-34 SF medium	ThermoFisher Scientific	Cat# 10639011
Propidium Iodide	ThermoFisher Scientific	Cat# P3566
TrypLE Express	ThermoFisher Scientific	Cat# 12605010
Fetal bovine serum, heat inactivated	ThermoFisher Scientific	Cat# 10438026
Bovine serum albumin	MilliporeSigma	Cat# A9576
Mouse Leukemia Inhibitory Factor	MilliporeSigma	Cat# ESG1106
Human transferrin	MilliporeSigma	Cat#T8158
L-Ascorbic acid	MilliporeSigma	Cat#S4544
EmbryoMax 0.1% Gelatin Solution	MilliporeSigma	Cat#ES-006-B
CHIR99021	Reprocell	Cat# 04–0004-10
PD0325901	Reprocell	Cat# 04–0006-10
Human basic FGF	R&D systems	Cat#233FB
Human BMP4	R&D systems	Cat#314BP
Human Activin A	R&D systems	Cat#338AC
Mouse VEGF	R&D systems	Cat#484MV
ZD6474	SelleckChem	Cat#S1046
Normocin	InvivoGen	Cat# ant-nr-1
Critical commercial assays		

Author Manuscript Author Manuscript Author Manuscript Author Manuscript

REAGENT or RESOURCE	SOURCE	IDENTIFIER
MethoCult M3434	StemCell Technologies	Cat#03434
NucleoSpin RNAII kit	Takara	Cat#740955.50
one-step SYBR Green PCR master mix	Bio-Rad Laboratories	Cat#1725150
Illumina TruSeq RNA Sample prep kit v2	Illumina	Cat #RS-122–2001
Fixation/permeabilization kit	BD Biosciences	Cat# 554714
Deposited data		
RNA- and ATAC-seq data	This paper	GSE136692
Experimental models: Cell lines		
Mouse: ZX1 embryonic stem cell	Laboratory of Michael Kyba	N/A
Mouse: Bry-GFP embryonic stem cell	Laboratory of Gordon Keller	N/A
Mouse: Etv2-tdTomato embryonic stem cell	Laboratory of Kyunghee Choi	N/A
Oligonucleotides		
qPCR primer: Mus musculus Nkx2–5 F: 5'- ACATTTTACCCGGGAGCCTA-3'	This paper	N/A
qPCR primer: Mus musculus Nkx2–5 R: 5'- GGCTTTGTCCAGCTCCACT-3'	This paper	N/A
qPCR primer: Mus musculus Bra (T) F: 5'- CCGGTGCTGAAGGTAAATGT-3'	This paper	N/A
qPCR primer: Mus musculus Bra (T) R: 5'- CCCCGTTCACATATTTCCAG-3'	This paper	N/A
qPCR primer: Mus musculus Isl1 F: 5'- TCATCCGAGTGTGGTTTCAA-3'	This paper	N/A
qPCR primer: Mus musculus Isl1 R: 5'- TTCCTGTCATCCCCTGGATA-3'	This paper	N/A
qPCR primer: Mus musculus Etv2 F: 5'- GCCGGGAATGAATTATGAGA-3'	This paper	N/A
qPCR primer: Mus musculus Etv2 R: 5'- CCCGAAGCGGTATGTGTACT-3'	This paper	N/A
qPCR primer: Mus musculus Scl/Tal1 F: 5'- gaggtcctaaccagccgagt-3'	This paper	N/A
qPCR primer: Mus musculus Scl/Tal1 R: 5'- cgtcctgtccctctagttgc-3'	This paper	N/A
qPCR primer: Mus musculus *Runx1* F: 5'- TTTTCGAAAGGAAACGATGG-3'	This paper	N/A
qPCR primer: Mus musculus *Runx1* R: 5'- TGGCATCTCTCATGAAGCAC-3'	This paper	N/A
qPCR primer: Mus musculus *Gapdh* F: 5'- TGTGTCCGTCGTGGATCTGA-3'	This paper	N/A
qPCR primer: Mus musculus *Gapdh* R: 5'- GATGCCTGCTTCACCACCTT-3'	This paper	N/A
qPCR primer: Mus musculus *Mesp1* F: 5'- GCTTCACACCTAGGGCTCAG-3'	This paper	N/A
qPCR primer: Mus musculus *Mesp1* R: 5'- GACTCAGGATCCAGGACTCG-3'	This paper	N/A
Software and algorithms		

Author Manuscript Author Manuscript Author Manuscript Author Manuscript

REAGENT or RESOURCE	SOURCE	IDENTIFIER
Flowjo	Flowjo, LLC	N/A
TopHat2 v2.1.1	Kim et al., 2013; Trapnell et al., 2009[60, 61]	https://ccb.jhu.edu/software/tophat/index.shtml
StringTie	Perteaetal., 2015, 2016[62]	https://ccb.jhu.edu/software/stringtie/
edgeR V3.16.5	McCarthy et al., 2012; Robinson and Smyth, 2007, 2008; Robinson et al., 2010; Zhou et al., 2014[63–67]	https://bioconductor.org/packages/release/bioc/html/edgeR.html
limma v3.30.13	Ritchie etal.,2015[68]	https://bioconductor.org/packages/release/bioc/html/limma.html
R V3.3.2	R Core Team	https://www.r-project.org/
Bowtie2 v2.3.0	Langmead and Salzberg, 2012[69]	https://github.com/BenLangmead/bowtie2
SAMtools v0.1.19	Li et al., 2009; Li, 2011[70, 71]	https://github.com/samtools/
MACS2	Feng et al., 2012; Zhang et al., 2009[72, 73]	https://pypi.org/project/MACS2/
deepTools	Ramirez et al., 2016[74]	deeptools.readthedocs.io
BedTools	Quinlan and Hall, 2010[75]	bedtools.readthedocs.io
preprocessCore v1.36.0	Bolstad et al., 2003[76]	bioconductor.org/packages/release/bioc/html/preprocessCore.html
TOBIAS	Bentsen et al., 2020[77]	https://github.com/loosolab/TOBIAS
Metascape	Tripathi et al., 2015; Zhou etal., 2019[78, 79]	metascape.org
MEME suite v5.0.5	Grant et al., 2011[80]	meme-suite.org
Seurat v4.0.0	Haoetal., 2021; Stuart et al., 2019; Butler et al., 2018; Satijaetal., 2015[81–84]	satijalab.org/seurat